

Millimeter-wave imaging of magnetic fusion plasmas: technology innovations advancing physics understanding

Y. Wang¹, B. Tobias^{2,6}, Y.-T. Chang¹, J.-H. Yu¹, M. Li¹, F. Hu, M. Chen¹, M. Mamidanna¹, T. Phan¹, A.-V. Pham¹, J. Gu¹, X. Liu¹, Y. Zhu¹, C.W. Domier¹, L. Shi^{1,2}, E. Valeo², G.J. Kramer², D. Kuwahara³, Y. Nagayama⁴, A. Mase⁵, and N.C. Luhmann Jr¹

¹ University of California at Davis, Davis, CA 95616, United States of America

² Princeton Plasma Physics Laboratory, Princeton University, Princeton, NJ 08543, United States of America

³ Tokyo University of Agriculture and Technology, Koganei, Tokyo 184-8588, Japan

⁴ National Institute for Fusion Science, Toki 509-5292, Japan

⁵ Kyushu University, Kasuga, Fukuoka 816-8580, Japan

⁶ Los Alamos National Laboratory, Los Alamos, NM 87545, United States of America

E-mail: ncluhmann@ucdavis.edu

Received 16 November 2016, revised 6 January 2017

Accepted for publication 3 February 2017

Published 14 March 2017



CrossMark

Abstract

Electron cyclotron emission (ECE) imaging is a passive radiometric technique that measures electron temperature fluctuations; and microwave imaging reflectometry (MIR) is an active radar imaging technique that measures electron density fluctuations. Microwave imaging diagnostic instruments employing these techniques have made important contributions to fusion science and have been adopted at major fusion facilities worldwide including DIII-D, EAST, ASDEX Upgrade, HL-2A, KSTAR, LHD, and J-TEXT. In this paper, we describe the development status of three major technological advancements: custom mm-wave integrated circuits (ICs), digital beamforming (DBF), and synthetic diagnostic modeling (SDM). These have the potential to greatly advance microwave fusion plasma imaging, enabling compact and low-noise transceiver systems with real-time, fast tracking ability to address critical fusion physics issues, including ELM suppression and disruptions in the ITER baseline scenario, naturally ELM-free states such as QH-mode, and energetic particle confinement (i.e. Alfvén eigenmode stability) in high-performance regimes that include steady-state and advanced tokamak scenarios. Furthermore, these systems are fully compatible with today's most challenging non-inductive heating and current drive systems and capable of operating in harsh environments, making them the ideal approach for diagnosing long-pulse and steady-state tokamaks.

Keywords: electron cyclotron emission imaging, microwave imaging reflectometry, integrated circuit, digital beamforming, synthetic diagnostics, horn antenna array, liquid crystal polymer

(Some figures may appear in colour only in the online journal)

1. Introduction: ECEI and MIR as powerful microwave imaging diagnostic tools for fusion plasmas

Electron cyclotron emission imaging (ECEI) passively collects spontaneous emission at harmonics of the cyclotron frequency, ω_{ce} , and produces a 2D image of electron temperature,

T_e , for a poloidal cross-section of optically thick plasma [1–6]. It utilizes the fact that the cyclotron frequency in a tokamak depends on the major radius, leading to a 1:1 mapping between emission intensity and the local T_e value. Along the poloidal direction, T_e is imaged onto a vertically aligned array of antennas. Figure 1 illustrates both conventional 1D

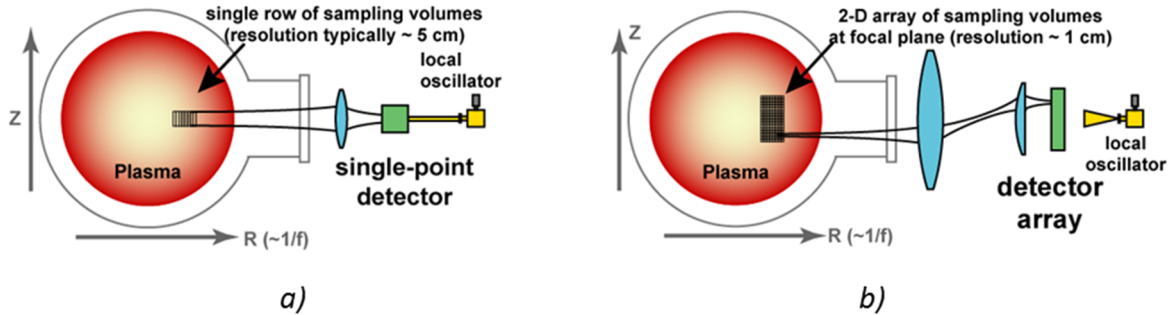


Figure 1. Conventional ECE radiometry and ECEI. (a) 1D temperature detection using a single-point detector; (b) 2D temperature profile obtained by a poloidally aligned detector array.

ECE radiometry and ECEI. Microwave imaging reflectometry (MIR) is a radar technique employed to infer electron density, n_e , and electron density fluctuations by probing the density dependent plasma cutoff layer with an injected microwave beam [7–11]. The injected beam, or probing microwave source, is reflected back to a receiving antenna and mixed with a reference signal. MIR uses quasi-optical techniques to image the plasma cutoff layer onto the receiver array, thus restoring the integrity of the phase measurement.

The earliest implementations of the ECEI technique provided paradigm-shifting insights into the nature of MHD behavior on the RTP, TEXT, and TEXTOR tokamaks [12–20]. As one example, ECEI provided the first opportunity to resolve localized reconnection and the formation of a narrow heat conduction channel at the time of the sawtooth crash (shown in figure 2). This eliminated invalid models of the physical mechanism behind sawtooth reconnection and allowed research in this area to proceed toward more sophisticated studies involving pacing of sawteeth and controlling the size of the sawtooth crash.

Microwave imaging reflectometry (MIR) was conceived by Mazzucato [18, 21, 22] and explored as early as 1995 [23] as a solution to a fundamental problem in reflectometry: the interference of multiple reflections and scattered radiation that corrupt measurement of the reflected wave's phase, and hence distort the inferred spectrum of plasma turbulence. MIR uses quasi-optical techniques to image the plasma cutoff layer onto the receiver array, thus restoring the integrity of the phase measurement. Figure 3 schematically depicts the MIR approach. In analytic theory and synthetic diagnostic modeling, it is easy to understand the advantages of imaging in reflectometer systems. Imaging allows the detector to reconstruct the fluctuations at a localized position in the plasma. Without some degree of imaging, there is little that can be done to prevent corruption of the diagnostic signal. This principle is underscored by the sensitivity of MIR diagnostics and the great challenge of producing consistent, reliable, high-quality data.

Under conditions when MIR diagnostics have been properly aligned to an appropriately configured discharge, the data are strikingly clear and free of artifacts such as amplitude modulation or signal phase skips. Data collected with a very simple MIR diagnostic on TEXTOR [18] demonstrated high-quality quadrature phase plots (proof that interference from scattered radiation could be eliminated and an example

of ‘good’ reflectometer data) and directly diagnosed poloidal ExB flow through reconstruction of the turbulent dispersion diagram (a plot of fluctuation frequency versus wavenumber).

2. Background: technological and physics advancements for ECEI and MIR

ECEI systems were installed on the ASDEX-Upgrade, DIII-D, EAST, J-TEXT, and KSTAR tokamaks during the period 2010–2016 and represent the current state-of-the-art [2, 24–39]. Refinements to the optical design, new imaging array configurations, and the use of automated fabrication for improved reliability of low frequency components allowed the technique to probe new phenomena. Diagnosis of Alfvén eigenmodes (shown in figure 4), their 2D and 3D mode structure, and the dependence of this structure on plasma parameters has advanced research in the areas of energetic particle (EP) driven instability and EP confinement in high-performance regimes. Plasma simulation codes could be compared with experimental data and improved with unprecedented efficiency. This had a major impact on multi-code validation studies and produced many widely-cited publications. Furthermore, it has allowed EP research to advance into a new generation of predictive capability and discharge scenario optimization. ECEI data are now routinely integrated into the identification of Alfvénic modes by comparison to modeling and the design of suppression techniques based on modeling validated by detailed 2D/3D images.

When conditions are favorable, as they often are on ASDEX-Upgrade and KSTAR, ECEI produces tantalizing images of ELMs and pedestal fluctuations (see figure 5). Results from ASDEX-Upgrade have provided considerable insight into the poloidal propagation of turbulence, peeling-balloonning modes, and detached filaments. This, of course, is indicative of the evolving radial electric field, an important element of nonlinear MHD behavior. On KSTAR, the changes in mode structure that accompany RMP ELM mitigation and suppression are compared with MHD simulation codes to infer changes in pedestal structure and disentangle the complicated nonlinear impact of 3D fields on transport and MHD stability. Again, these data have a significant impact on fusion research and promise to have an even greater impact as the new technology described in section 3 will allow similar data to be obtained under increasingly ITER-relevant conditions.

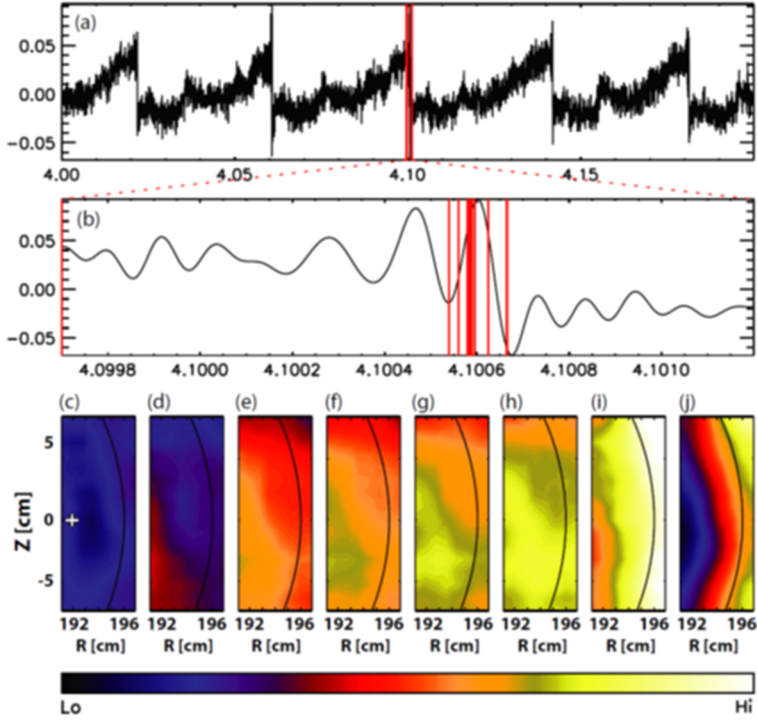


Figure 2. Sawtooth waveform of the repeating growth/crash cycle (a), zoom of single crash event (b) and sequence of 2D ECEI images of the temperature fluctuations corresponding to indicated time points ((c)–(j)). The color scale runs from +10% to –7% of the time average. The arc in the images ((c)–(j)) indicates the $q = 1$ surface. Waveforms (a) and (b) correspond to the location indicated by the cross in image (c). Reproduced courtesy of IAEA. Figure from [6]. Copyright 2007 IAEA.

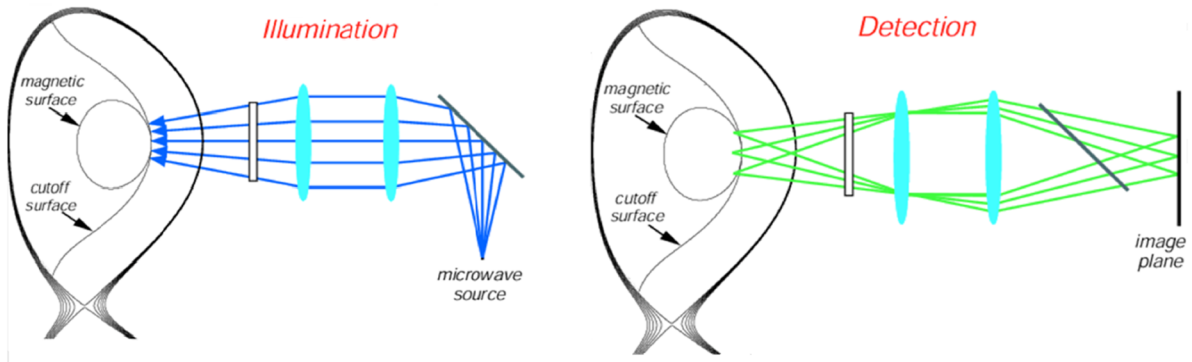


Figure 3. The principles of operation for MIR reflectometry. First, the probing beam illuminates an extended region of the cutoff layer, where the curvature of the illuminating beam is matched to that of the cutoff surface (both toroidal and poloidal). Then, the cutoff layer is imaged onto a detector array at the image plane (3 example points shown), thereby eliminating the interference effects of multiple reflections. The illumination and detection systems share the common plasma-facing optics.

For example, DIII-D, with an excellent suite of complementary profile diagnostics (edge Thomson scattering, impurity and main ion CER, etc.) allows possibly the most sophisticated experiments to be performed and readily coupled with computational modeling. However, the low-collisionality of DIII-D H-mode and QH-mode plasmas, while very attractive for reproducing ITER-like conditions, also leads to bursts of radiation (often saturating the diagnostic at more than 100 times the radiation temperature of the background plasma) that are challenging for microwave diagnostics. These mm-wave bursts have been documented in some detail on DIII-D, C-Mod, MAST, and even in the very lowest collisionality discharges produced on ASDEX-Upgrade, but have not been

fully described by theory or plasma simulation [41–48] with suggested explanations ranging from coherent radiation due to the collective behavior of electrons in the pedestal as they interact with periodic modulations of the magnetic field associated with MHD mode to the presence of suprathermal, magnetic-field-aligned electron populations that drive waves in the EC range via the anomalous Doppler instability (ADI). Upgrading the DIII-D ECEI diagnostic will (1) reject out-of-band interference to produce the cleanest possible images, and (2) better resolve bursts which are within the bandwidth of the diagnostic, allowing them to be separated from the underlying MHD mode structure and studied in detail.

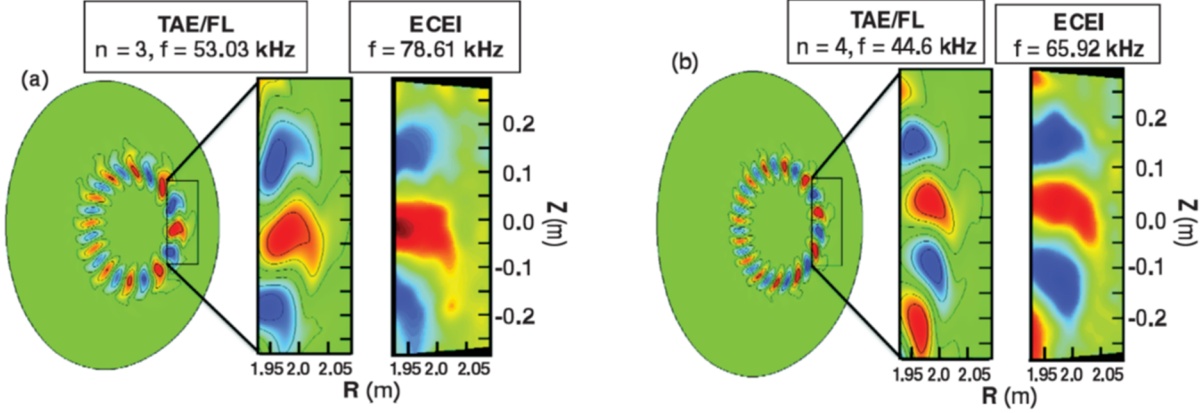


Figure 4. Imaging of RSAEs near $t = 725$ ms reveals shearing of the Alfvén eigenmode structure which cannot be described by the ideal MHD approximation. In the (a) $n = 3$ and (b) $n = 4$ modes shown, the fluctuation phase reveals an outward spiraling, or poloidal shearing, of the mode in the ion diamagnetic drift direction. This behavior is well represented in the nonperturbative code TAEFL, where the effect of fast-ion dynamics is included in the 2D eigenmode structure. A discrepancy in mode frequency arises from the omission of compressibility in the simulation model and is found to be consistent with the geodesic acoustic shift of the Alfvén continuum. Reprinted figure with permission from [40] Copyright 2011 by the American Physical Society.

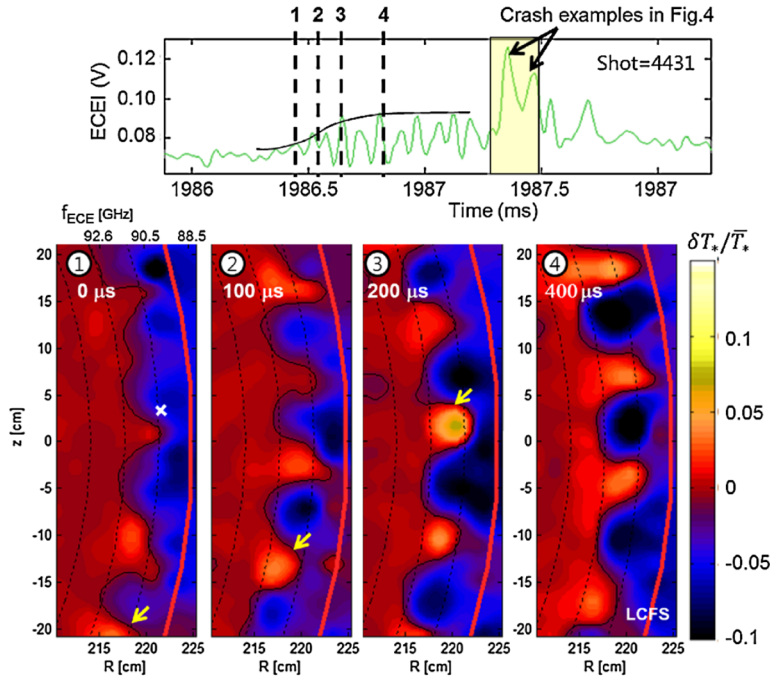


Figure 5. Simultaneous emergence and growth of multiple ELM filaments (shot no. 4431). Solid curves are contour lines of the same $\delta T^* / \bar{T}^*$ value representing the approximate boundary of the filaments. The arrows follow the same filament illustrating the counterclockwise rotation. Reprinted figure with permission from [49] Copyright 2011 by the American Physical Society.

A considerably more refined implementation of MIR was deployed on DIII-D in May 2013 and began taking plasma data in July 2013 [10]. This diagnostic had significantly improved antennas and quasi-optical components for better coupling to the plasma, higher power sources for improved probing of the cutoff surfaces, and implemented a number of new microwave techniques to stabilize the system and isolate the reflected signal. This diagnostic has produced exciting 2D images of edge fluctuations and contributed to the investigation of QH-mode physics (see figure 6) and has successfully diagnosed core Alfvén eigenmodes. However, robust diagnosis of 2D mode structures with changing and/or unpredictable

plasma conditions requires a more active approach to aligning, acquiring, and tracking the discharge. This is the motivation for pursuing the advanced beamforming techniques described in section 4, which will impact reflectometry more broadly, by prescribing methods that allow reflectometer data to be interpreted with a much higher degree of confidence.

A major issue confronting current tokamak ECEI systems is that noise and interference hampers efforts to image ELMs under low-collisionality conditions like those on DIII-D during ITER baseline scenario studies and which has limited measurements during LHCD on EAST. Additionally, fast and robust imaging of core and edge fluctuations, including ELMs

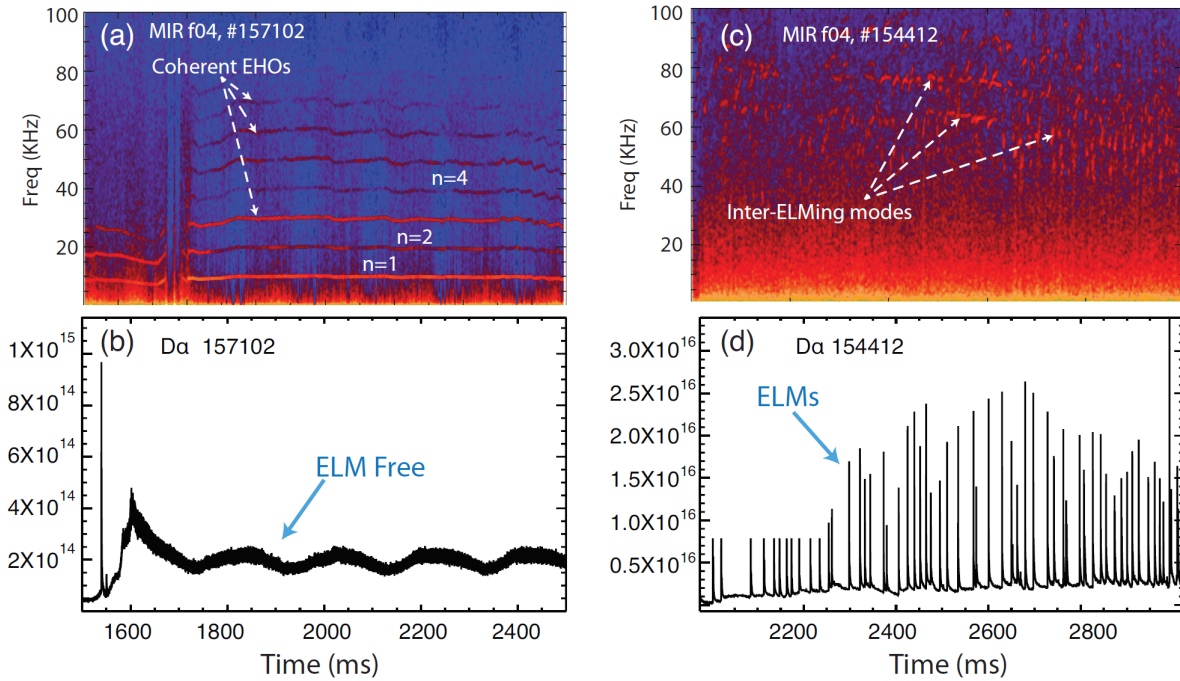


Figure 6. Examples of quiescent H-mode (left) and conventional H-mode (right). The quiescent H-mode has strong coherent EHOs measured with MIR (upper left), and no bursts of Da radiation at the divertor (lower left). The conventional H-mode is ELMing with frequent spikes of Da emission (lower right). MIR measured inter-ELMing modes has higher frequencies (upper right) for conventional H-mode. Reproduced from [50]. © IOP Publishing Ltd. CC BY 3.0.

and AEs, are difficult to achieve because current ECEI and MIR systems employ motor-controlled optical lenses that are positioned to provide focusing for particular plasma conditions essentially once per discharge.

To this end, we have pursued three major transformative technological advancements for fusion plasma diagnostics: in particular, custom mm-wave integrated circuits (ICs), digital beamforming (DBF), and synthetic diagnostic modeling (SDM), for MIR, ECEI, and a host of other microwave diagnostic techniques that rely on the same functional sub-system [51]. IC technology facilitates the use of a horn waveguide array configuration such as developed by Kuwahara *et al* for ECEI and MIR and implemented on LHD [52–55] which significantly eliminates interference through the shielding and fundamental waveguide transition (>100 dB for LHCD stray microwaves below 5 GHz). The IC technology reduces noise temperature (down to 627 K at 100 GHz and 1340 K at 220 GHz), which enables absolute calibration and simplifies system setup, which in turn facilitates operation in harsh environments. DBF allows finely-tuned alignment that tracks changing conditions in real time, thereby facilitating studies including disruption precursors. When complemented by new software and advanced SDM capabilities [56–60], these technologies will enable compact and low-noise transceiver systems with real-time, fast tracking capability (as shown in figure 7) to address critical fusion plasma physics issues, including the ITER baseline scenario [61–63] and QH-mode [50, 64–66]. For each development, the advanced technology finds immediate application as ‘plug-in’ modules, which can be integrated into existing mm-wave imaging systems to provide enhanced capability. Furthermore, it will do so more reliably and at lower cost, maximizing scientific productivity in the process.

This paper consists of a review of the recent hardware and software development for fusion plasma diagnostics carried out by UC Davis and PPPL together with collaborators at NIFS, Kyushu University, and Tokyo University of Agriculture and Technology. Sections 3 and 4 provide background information concerning the fundamental technological aspects of ICs and DBF, respectively. Progress and accomplishments are presented, including the prototypes and current upgrade of the common receiver architecture for ECEI and MIR, customized CMOS transmitter IC for MIR, and digitally controlled electronic phase shifter for steerable phased arrays. Section 5 presents the progress for the forward 2D/3D full-wave modeling of the plasma-wave interaction for reflectometry. The use of synthetic diagnostics for forward modeling of the instrument response is discussed. Finally, the technological trend and development road maps are presented in section 6.

3. Custom microwave circuit integration

3.1. Mm-wave integrated circuits (ICs)

IC technology facilitates combining many bulky microwave components onto a single, tiny piece of semiconductor substrate. Such a compact ‘system-on-chip’ (SoC) can be inexpensively customized for fully optimized instruments. For example, it has been the key enabling factor for compact and sensitive wireless transceiver systems in radar, satellites, and cellular phones, which are ubiquitous in the modern telecommunication and sensor industry [67–69]. Likewise, IC technology will bring transformative advances in microwave fusion plasma diagnostics. Current microwave imaging diagnostics are compromised by strong environmental noise

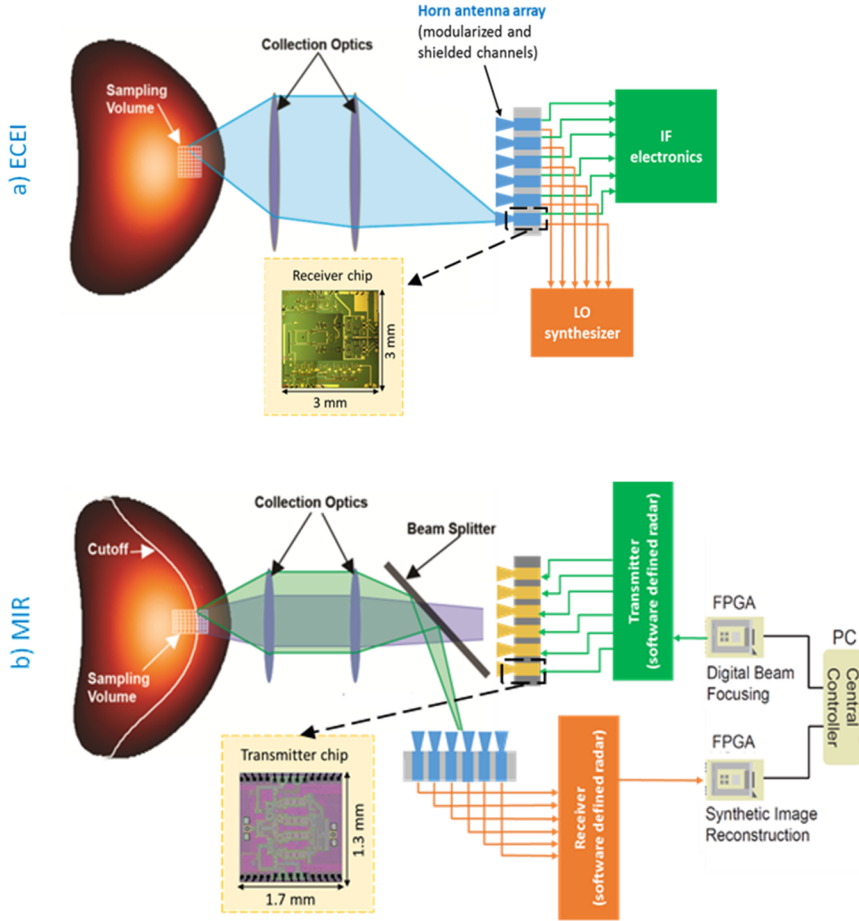


Figure 7. Advancements for ECEI and MIR. (a) Circuit integration eliminates the noise and interference that has frustrated efforts to image ELMs under low-collisionality conditions like those on DIII-D during ITER baseline scenario studies; (b) digital beamforming allows alignment to be fine-tuned, even feedback-controlled, for robust imaging of core and edge fluctuations including ELMs and AEs.

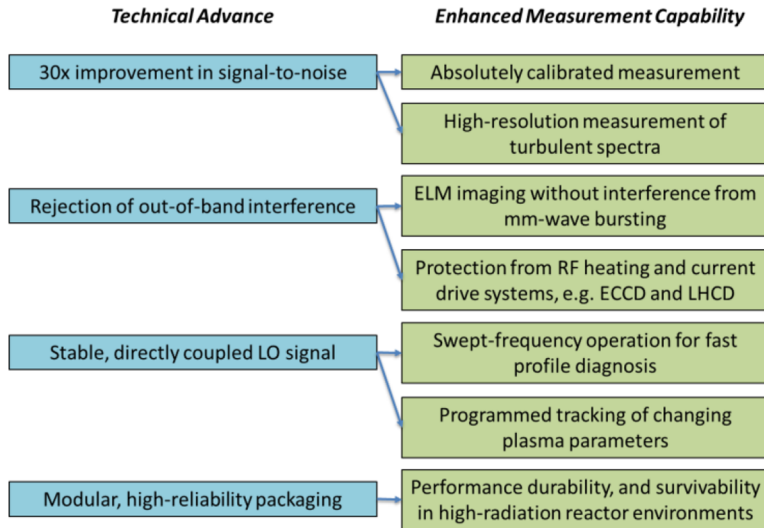


Figure 8. IC development enables measurements that have been difficult or impossible to date, using the current state-of-the-art ECEI instruments that directly employ a single-ended Schottky diode mixer for signal down-conversion. Reducing receiver noise temperature will simplify the absolute calibration process by allowing lower temperature references to be used with shorter integration times. Delivering LO power to the mixer directly and without free-space optical coupling provides a further range of valuable benefits, ultimately providing the high-resolution imaging of the plasma edge that for existing systems is easily corrupted by interference and instrumental uncertainties.

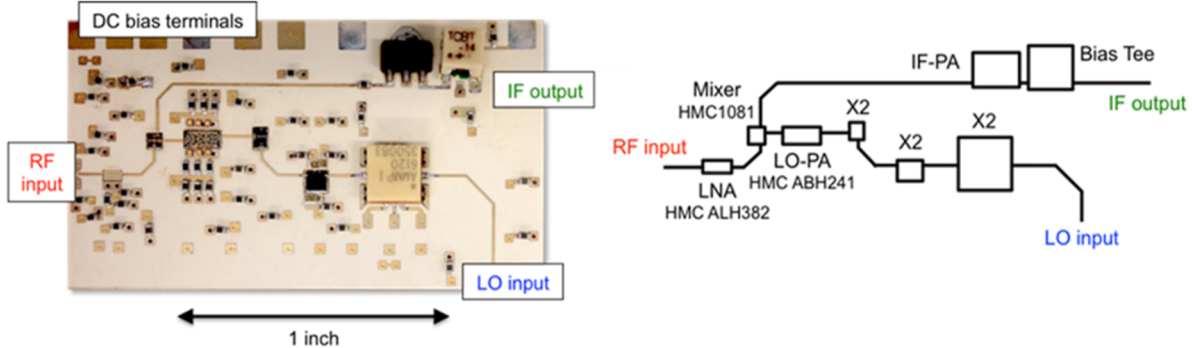


Figure 9. A single-channel heterodyne GaAs MMIC based receiver circuit on LCP substrate. Primary components of the circuit are shown.

and the inefficiency of signal mixing and down-conversion. As shown in figure 8, features such as significantly improved noise rejection, stability, and circuit protection will enable new measurement capability with absolute calibration, fast swept profile information, and unprecedented performance and survivability in harsh, high-radiation reactor environments.

An important aspect of IC technology is the way in which it transforms a microwave diagnostic. In many state-of-the-art systems, each device-level function is performed by a separate component, each of which is purchased at considerable expense from a commercial vendor, already packaged and connectorized. Diagnosticians then typically assemble a functional instrument by simply connecting these packages together with short sections of fundamental waveguide resulting in the common expression of microwave waveguide ‘plumbing’. In doing so, compromises must be made in order to physically arrange the bulky packaged components, match one component’s gain to another’s input power handling, etc. Since most of the components are designed with a completely different application in mind (e.g. radar or communications), the diagnostician is dependent upon market forces unrelated to fusion such as an ever-changing product catalog and costly vendor warranties. Where the specializations of fusion diagnostic applications are concerned, antennas and quasi-optical local oscillator (LO) coupling schemes have to be devised ad-hoc and integrated, sometimes with great difficulty. A custom IC, on the other hand, is a game-changer; one tiny chip can contain all the essential circuit elements, perfectly optimized for fusion application. A single specialized package can be fabricated around this chip to include an optimized antenna, a minimum number of low frequency inputs/outputs, and a completely shielded power supply. Furthermore, the IC itself can be mass-produced, making for a bench-stock of consistent and yet inexpensive replacement circuits that can be swapped out with minimal effort—clearly an advantage in fusion where experimental resources and run-time are at a premium!

3.2. Transformation of ECEI and MIR common receiver architecture

A critical component enabling ECEI and MIR is the heterodyne imaging array that collects and down-converts radiated emission and/or reflected signals (currently 50 to 150 GHz)

to an intermediate frequency (IF) band (e.g. 0–18 GHz) that can be transmitted by shielded coaxial cable to additional modules for further filtering and detection. New front-end circuitry based on the ‘system-on-substrate’ topology shown in figure 9, has been developed for this task [69]. Compared to the current state-of-the-art receiver system, this new design offers both device and system-level advancements. On the device level, the receiver employs commercially available gallium arsenide (GaAs) MMICs, which offer low-noise (below 850 K at 80 GHz) and high gain (>20 dB) performance compared to the current single-Schottky diode mixer based systems. On the system level, it employs liquid crystal polymer (LCP) as the integration substrate with excellent electrical and mechanical properties [70–74].

One striking advantage of this approach is the resulting simplification of the system layout as shown in figure 10—the reduction of real-estate required for an ECEI or MIR diagnostic. In the case of ECEI on DIII-D, the on-board LO eliminates the need for nearly 40 meters of low-loss, corrugated waveguide and eliminates the vacuum tubes (BWOs) used to generate high-frequency LO power.

Current tokamak imaging systems, like that shown in figure 11, consist of Schottky diodes mounted on printed antennas with dielectric substrate lenses (visible in figure 11(a)). These lenses are mounted inside a conducting box; however, large apertures are necessary to optically couple LO power and the radiation from the plasma. Considerable effort is made to isolate the antennas from stray radiation, including the use of dichroic plates, but this has proven to be of limited utility. With so much system gain, even a tiny amount of stray radiation (such as from a wireless computer network router) can overwhelm the signal. In addition, there are numerous opportunities for leakage, such as the couplings of discrete amplifiers and power supplies (see figure 11(b)). In contrast, the system-on-substrate approach allows the entire receiver to be packaged in a hermetically sealed structure that not only performs better, but is more compact, more reliable, and far simpler to service in the worst case scenario of microchip failure.

Of equal importance is the impact of an improved architecture on system performance and data quality. As noted above, the existing ECEI and MIR receiver systems employ a single-ended diode mixer directly at the antenna for RF signal down conversion. In contrast, the new receiver approach places a

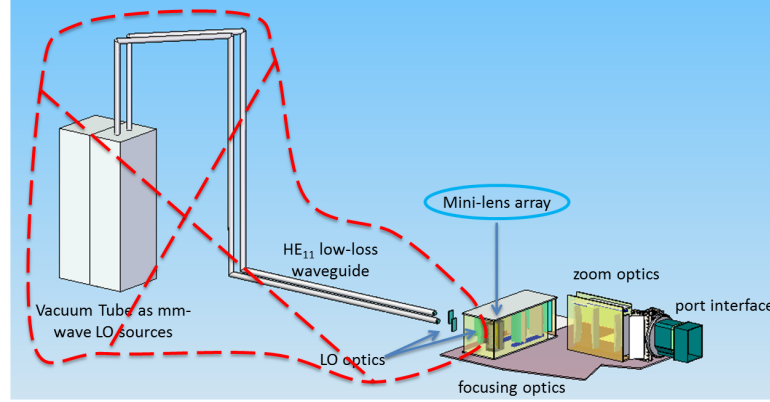


Figure 10. The LO signal generation and guiding in the current system. The mini-lens array (blue circle) is replaced by the horn antenna array. The vacuum tube LOs, HE₁₁ corrugated waveguide, and the LO optics (red circle) are completely eliminated.

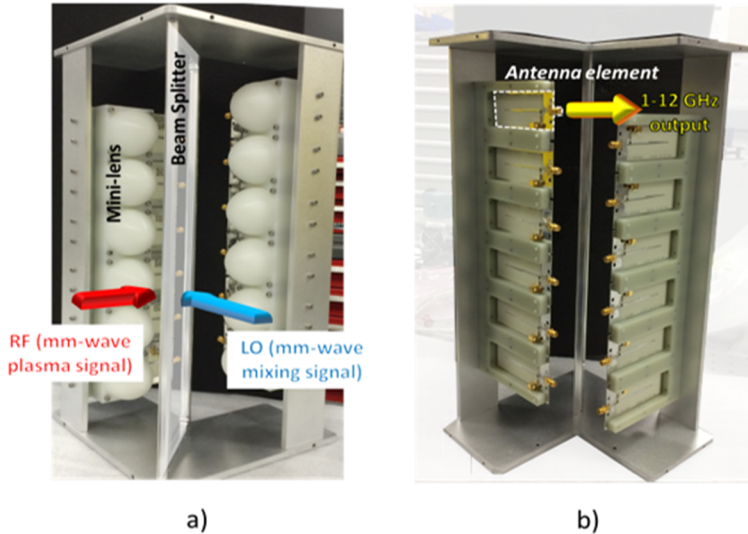


Figure 11. An example of the current receiver array configuration: the elliptical dielectric mini-lenses visible in part (a) conceal printed dipole antennas upon which the mixing element, a simple Schottky diode, is directly mounted. This structure must have a large aperture line of sight for optical coupling of plasma radiation and LO power, making the high-gain circuit extremely susceptible to out-of-band radiation. The rear of the antenna array shown in part (b) must also be shielded from stray radiation and interference while accommodating low-noise amplifiers and DC bias circuitry. Sufficiently isolating this structure from interference has proven challenging, severely limiting the quality of ECEI and MIR data.

low-noise amplifier (HMC-ALH382 by Analog Devices, Inc. with 5 dB noise figure) before a balanced mixer, which significantly improves electromagnetic isolation from out-of-band interference, and leads to 10× improvement in the signal-to-noise ratio compared to the current ECEI receiver. This signal-to-noise ratio can be further increased to 30× if a single GaAs system-on-chip (SoC) receiver is utilized instead of integrating the receiver system-on-substrate with individual MMICs. The noise temperature comparison between the current and new heterodyne architecture is quantified in figure 12. The benefit, beyond improved out-of-band rejection and compactness, may not be immediately obvious since the receiver noise temperature is considerably less than the non-thermal electron temperature fluctuations of interest which, in turn, are significantly smaller than the radiation temperature fluctuations. This has motivated the development of a variety of correlation techniques to recover nonthermal fluctuations [19, 75, 76] and which provide local, normalized temperature

fluctuations. However, the integrated receiver chips have sufficiently low noise temperature that an absolute hot–cold load calibration of the entire system is possible and thus absolutely calibrated temperature profiles may be obtained, thereby significantly expanding the capability of the instrument.

As mentioned previously, the horn-waveguide approach provides considerable out-of-band rejection (>100 dB at 5 GHz). However, there is still the question of stray radiation within band. To assess the protection level required, we note that the 65 nm CMOS devices can safely operate under 10 dBm input power. For GaN low noise amplifiers, we expect that the input power can be as high as ~20 dBm in the W-band [77] and ~10 dBm in G-band [78]. However, these LNAs can be protected with limiters which are widely used in phased-array antenna systems. For our systems, a number of techniques [2] such as notch filters (up to 60 dB rejection), novel fuses, and limiters can be used to protect the LNAs. For on-chip or fully integrated circuits, limiters are widely used for protection of receivers with InP and

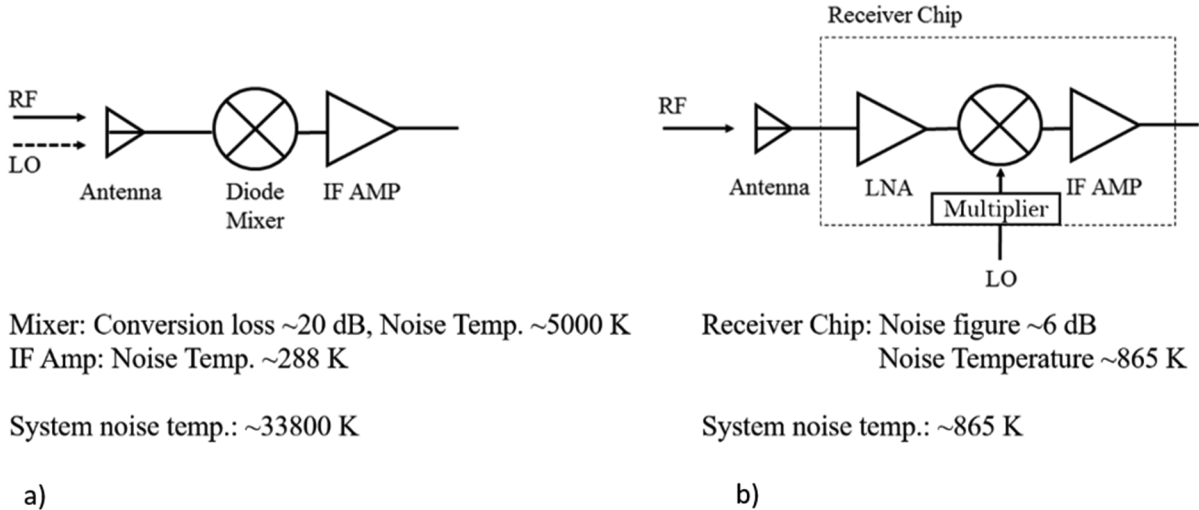


Figure 12. Comparison of the heterodyne receiver architecture in the current ECEI and MIR systems and the advanced system. (a) The current receiver architecture suffers from the large conversion loss of the diode mixer, which leads to very high system noise temperature by multiplying the temperature of the IF amplifier by the conversion loss. (b) The new system utilizes an LNA in front of the mixer, which helps to reduce the system noise temperature by a factor of 30 permitting absolute *in situ* calibration and microturbulence fluctuation studies, and generates the millimeter wave LO on-chip eliminating the need for quasi-optical combining of RF and LO signals resulting in a small, highly-shielded array.

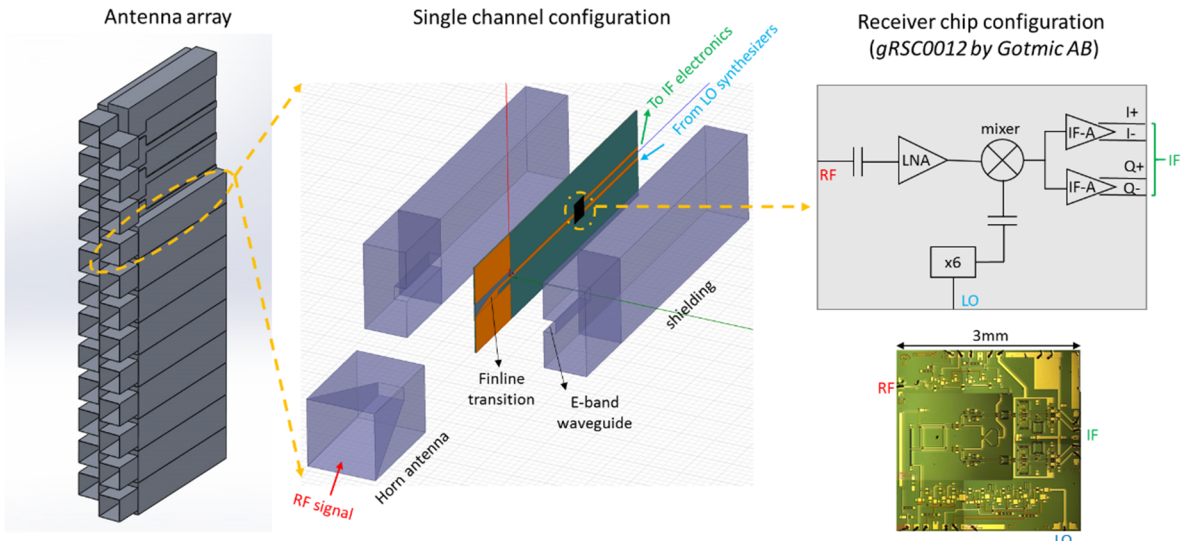


Figure 13. RF and LO mixing configuration in the horn waveguide system. Each channel is completely modularized and shielded. The E-band GaAs chip consists of a complete receiver front-end, which occupies an area of only 3 mm × 3 mm.

GaN devices able to provide limiter circuits capable of handling a few watts input power to protect the LNA in the W-band and ~1 W in the G-band (up to 220 GHz).

A proof-of-principle design, optimized for reflectometry and edge radiometry on mid-sized tokamaks, has demonstrated >20 dB conversion gain in V-band (60–75 GHz) in the laboratory. Implementation of the circuit in a multi-channel ECEI waveguide horn array configuration as developed for LHD [52–55] will improve the diagnosis of edge-localized modes and fluctuations of the high-confinement, or H-mode, pedestal. However, the availability of individual commercial MMICs covering the frequency range of interest for current tokamaks is limited. Integration and packaging at such high frequencies also introduce additional challenges and losses.

These issues are solved with system-on-chip integration of the heterodyne architecture, where the entire receiver is fabricated on a single chip and each building block is optimized and matched at the frequency of interest. SoC integration delivers the advantages of on-board LO delivery and eliminates packaging losses as well as further reducing noise temperature (from 10× reduction to 30×). This approach is being demonstrated through a DIII-D ECEI system upgrade illustrated in figure 13, where commercially-available chip receivers produced by Gotmic AB in Sweden are employed. Although these are limited to the E-band designation (71–76 GHz), a strategy has been developed for compensating their performance over a slightly wider range (70–80 GHz) so that they will support ELM imaging in the most common ITER 15

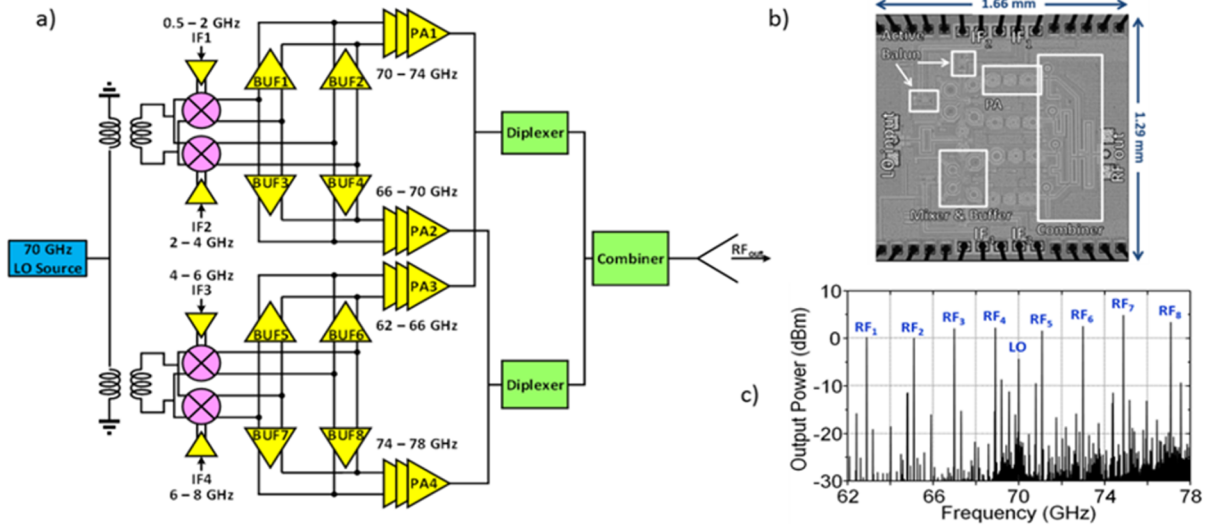


Figure 14. The V-band 8-tone CMOS transmitter IC. (a) System architecture; (b) layout and footprint of the chip ($1.66\text{ mm} \times 1.29\text{ mm}$); (c) measured result of the 8 tone output power.

MA scenario development discharges on DIII-D. Diagnosing ELM structure in those discharges has been frustrated by high-power bursts of microwave emission near the ELM times—power that saturates the diagnostic and corrupts the image [41, 43]. These and similar bursts have been observed on DIII-D, EAST, ASDEX-Upgrade, and even MAST [47], and are interesting in their own right; they occur at ITER-relevant collisionality and have damaged diagnostic systems in the past (e.g. the ORNL Q-band SOL reflectometer on DIII-D). We believe that much of the power is radiated outside the primary band of the ECEI diagnostic and therefore are confident that ELM imaging will be improved by greater out-of-band rejection through SoC integration.

The upgraded ECEI system will significantly surpass the current state-of-the-art ECEI imaging array. In the package illustrated in figure 13, each channel is completely modularized and individually shielded. A horn antenna array (17 dB gain to replace the existing DIII-D ECEI low-field mini-lens array without changing any of the rest of the optics) with fundamental waveguide transitions provides enormous attenuation for out-of-band interference (>100 dB for LHCD stray microwaves below 5 GHz) [53]. In addition, there are only a limited number of low-frequency and DC power connections required. These features are critical for eliminating the mm-wave bursting that has contaminated ELM data in the most interesting and most ITER-relevant low-collisionality regimes, allowing for a wealth of new images to be obtained and facilitating a wide range of pedestal stability studies. It also provides a path forward for high-quality imaging on steady-state tokamaks such as EAST where RF heating systems such as ECCD and LHCD pose an enormous challenge for the current state-of-the-art. Finally, note that reduced noise temperature, combined with the fast-tuning capability that comes with using a low-frequency synthesizer source to generate the LO power, allows the diagnostic to be operated as a calibrated, fast-sweeping profile diagnostic for high-resolution 2D characterization of the absolute electron temperature across the pedestal. In fact, new synthetic diagnostic

capabilities discussed briefly in section 5 have been developed with the prospect of this new measurement capability in mind.

3.3. High-power, multi-tone custom CMOS transmitter IC for enhanced DIII-D, EAST, and NSTX-Upgrade MIR diagnostics

The explosive growth of high-speed wireless communications has led to a proliferation of commercially available ICs, although often limited to specific applications (and thus frequencies) that do not cover the range for fusion plasma diagnostics. Therefore, developing customized ICs that are targeted specifically for fusion plasmas is imperative for developing optimized microwave imaging capabilities for comprehensive fusion physics studies.

To this end, we have successfully designed, fabricated, and tested a multi-frequency (8 tone) illumination transmitter IC chip based on the CMOS technology for simultaneously probing the radially dependent cutoff surfaces [79]. This represents a major step in developing customized ICs for fusion plasma diagnostics. It will be integrated in the upgraded DIII-D MIR system. The system architecture of the transmitter chip is illustrated in figure 14(a)), which features four mixers and four power amplifiers for double-sided up-conversion and power boosting at eight separate frequencies. Each output signal is optimized with a narrowband buffer and a power amplifier to maximize the gain and efficiency. The first working prototype of the CMOS multi-frequency transmitter has been fabricated which measures only $1.7\text{ mm} \times 1.3\text{ mm}$ (see figure 14(b)), and delivers more than 1 mW of power at each of 8 frequencies and is tunable from 62–78 GHz (see figure 14(c))⁵. The new system-on-chip (SoC) CMOS transmitter expands the capabilities of microwave reflectometry as a fusion plasma diagnostic while at the same time making systems dramatically less expensive, more compact, and more reliable. Currently costing less

⁵ For comparison purposes, the current DIII-D four frequency MIR transmitter provides 4.5 mW/frequency.

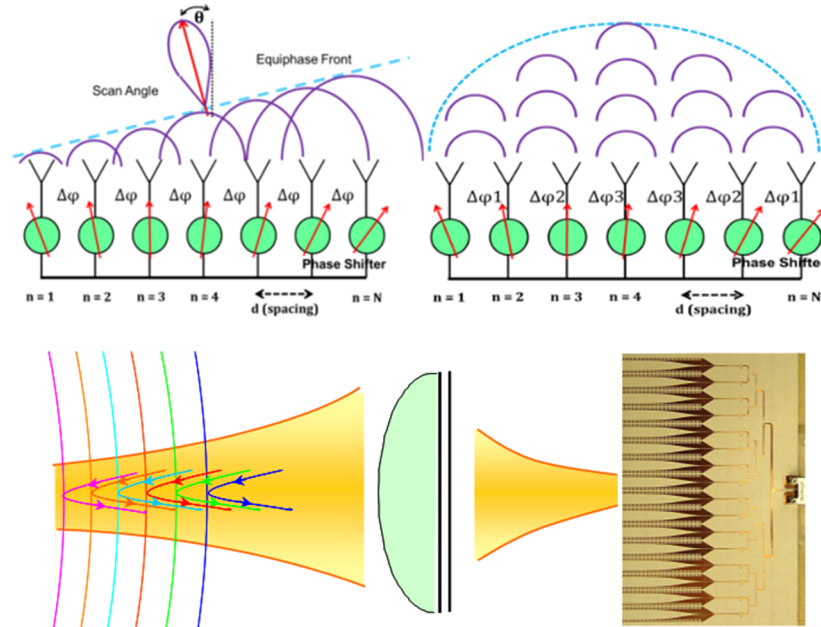


Figure 15. Phased arrays for beam shaping and steering, and their application in fusion plasma diagnostics.

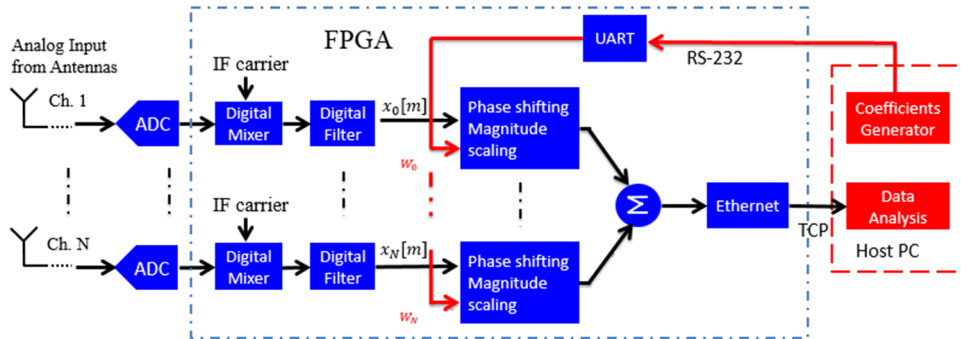


Figure 16. Diagram for digital beamforming receiver module employing an FPGA.

than \$50 to fabricate⁶, each SoC makes for a hot-swappable sub-system replacing as much as \$40 000 worth of discrete components. In the near future, further integration of the 2D microwave imaging reflectometer (MIR) will make for even greater cost savings.

4. Electronically and digitally controlled active focusing and alignment

4.1. Electronic and digital beamforming

Phased array and synthetic aperture technologies allow the antenna pattern (the field of view, viewing angle, focal length, and gain) to be controlled electronically or by digital processing, making for systems that are fast-tracking and remotely tunable without the need for bulky lenses and meticulous, slow, mechanical alignment. They are often comprised of multiple, identical radiators (shown in figure 15), where the far-field array pattern is the product

of each element's field pattern and the array's spatial factor. Intelligent design of these systems using the latest techniques can provide flexible systems with the low side-lobe levels required for imaging fusion plasmas, and enable the next generation of auto-tracking and feedback-controlled imaging diagnostics.

There are two major categories of phased arrays. One is the analog phased array where the phase shaping and steering are provided with analog phase shifters. Another approach that has advantages is digital beamforming (DBF), where the phase shifting and amplitude scaling are accomplished by mathematical operations in a low-frequency baseband. Compared to the traditional analog beamforming, digital beamforming is more accurate and allows faster control of the phase and amplitude. It also provides the ability to form multiple beams simultaneously.

A field programmable gate array (FPGA), as illustrated in figure 16, is used to generate digital control signals for phased array beam shaping and steering. It's a convenient, mature, and robust approach to achieve digital beamforming, and maintain active control of the optimal focusing with advanced algorithms. Analog signals coming from each

⁶In production mode, rather than R&D mode, this would drop to much less than \$1/chip.

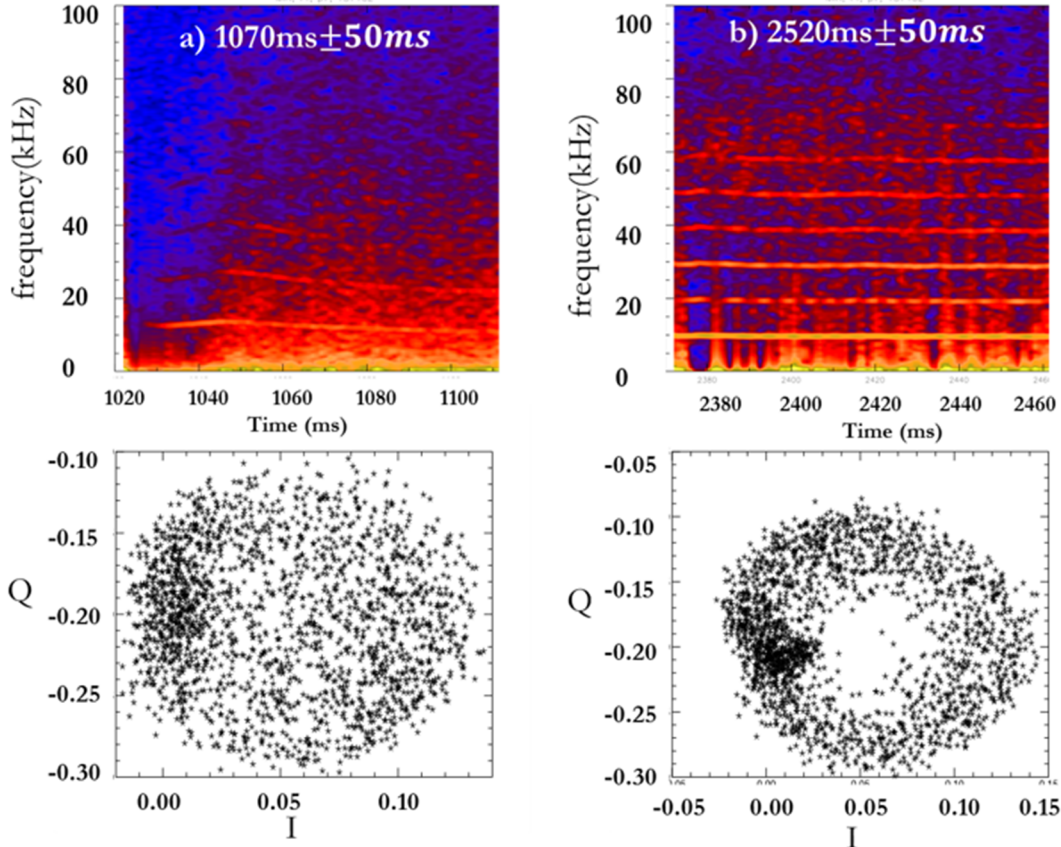


Figure 17. Two windows within the same discharge are shown to illustrate the importance of alignment in obtaining high-quality reflectometry data. In (a), the discharge is not well-aligned with the diagnostic and the data are indistinct with poor resolution of the fluctuation spectrum. These data are no better than those obtained by a conventional reflectometer without imaging optics. In (b), the discharge has evolved to an optimal shape and the improvement in data quality is evident from both the spectrogram and IQ plot: interference from scattered radiation is minimized, the amplitude of the received signal is more constant, and the signal phase is representative of the local density fluctuation. Fast, digital and electronic beamforming will allow this alignment to be fine-tuned in real time, with either pre-programmed or feedback-controlled algorithms.

channel of the antenna array are first digitized and mixed with the IF carrier frequency to retrieve the corresponding I/Q components. Beam shaping/steering coefficients are generated on the PC and sent to the FPGA through the universal asynchronous receiver/transmitter (UART) port. Each channel's signal (I/Q signal) is applied with a certain phase shift and magnitude scaling based on the corresponding coefficients (alternatively, the embedded processor on the FPGA can be employed for the coefficient generation). All the channels' signals are then summed together to provide the desired beam shape and direction. The results are then sent to the PC for further analysis through a high speed Ethernet connection.

For plasma diagnostic systems, actively maintaining optimal focus and alignment is critical to localizing the measurement, achieving adequate signal-to-noise ratio, and selecting the desired fluctuation wavenumber; it is essential for the robust diagnosis of density fluctuations, as shown in figure 17. Without proper alignment, scattered radiation interferes at the receiver, mixing both the amplitude and phase of the signal. The spectrum shown in part (a) is poorly resolved, and the raw signal, represented as temporal points plotted in a complex plane, is an

indistinct cloud. As the discharge evolves and comes into alignment with the diagnostic, as in part (b), the data cloud begins to form an annulus of time-dependent phase, but uniform amplitude. This is indicative of good coupling to the plasma cutoff surface, and the corresponding fluctuation spectrum becomes a clear representation of the local density fluctuation.

Intelligent control of the alignment in both pre-defined and real-time with electronic beam steering can solve problems in obtaining alignment between transmit and receive systems with accurate coupling of the plasma cutoff surfaces with active diagnostic feedback where the intrinsic DBF control is about 1 μ s and IQ plot identification requires ~0.20 μ s for 5 MHz sampling rate. In cases such as some physics scans where profiles are changed between discharges, the DBF coefficients can be pre-programmed. Figure 17 illustrates a case where active control is required. Here, there is a transition around 1550 ms over a timescale of 200 ms. The examination of the I-Q plots in figure 17 shows how they can be used in the correction algorithm. Therefore, phased-array antennas with digital beamforming capabilities are the key to characterizing, understanding, and monitoring scientifically interesting phenomena and important topics, such as tokamak disruptions.

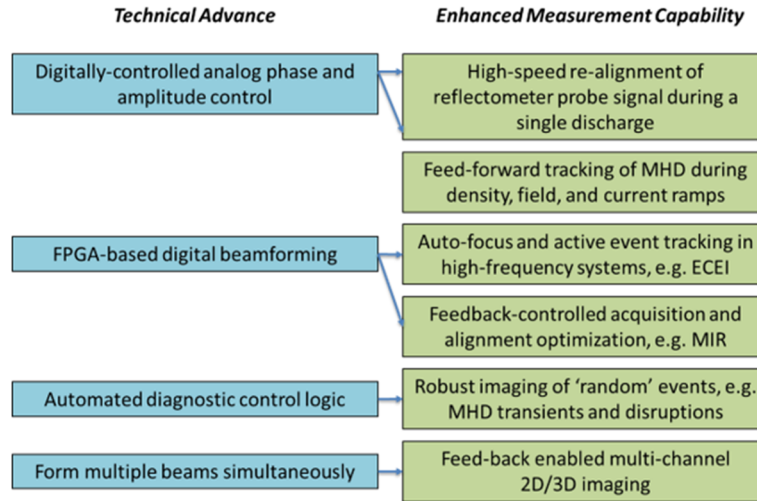


Figure 18. The FPGA enabled digital beamforming development facilitates fast, flexible, and reliable tracking of cutoff surfaces and data collection during a single plasma discharge.

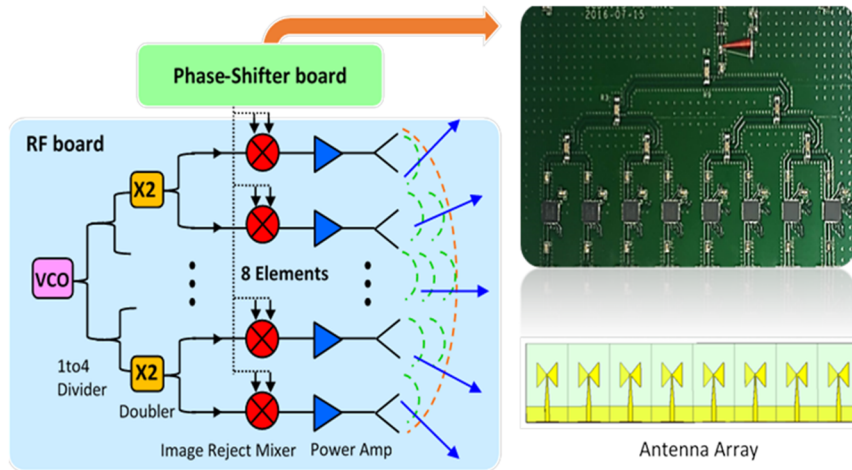


Figure 19. Block diagram of the electronically controlled phase shifter transmitter system.

The scientific benefit of this development is summarized in figure 18.

4.2. Phased arrays for digitally-controlled electronic beam steering and active tracking

Dynamically maintaining optimal focus and alignment is critical to localizing the measurement, achieving adequate signal-to-noise ratio, and selecting the desired fluctuation wavenumber. However, current reflectometry and radiometry systems are not able to provide such features because the antenna far-field radiation is controlled quasi-optically using dielectric lenses and/or mirrors. On the other hand, electronic phased arrays utilize multiple antennas to transmit/receive signals instead of a single radiator. Therefore, their far-field array pattern can be actively steered rapidly by controlling the phase offset for each constituent antenna through electronic phase shifters.

A digitally-controlled electronic phase shifter board has been designed and tested for employment in an eight-channel transmitter phased array to facilitate dynamic beamforming.

The block diagram of the transmitter phased array is shown in figure 19, where a photograph of the electronic phase shifter board is also presented. The system is comprised of eight channels, and the phase shifter chip in each channel is digitally controlled to provide desired phase offset from each other. The output signals from the phase shifter board are connected to the RF board, where further up-conversion and beamforming are facilitated. In this design, the signal phase from each channel can be controlled with 1.4° resolution and 360° full scan range.

5. Forward modeling the diagnostic response

5.1. Synthetic diagnostics

Synthetic diagnostics are advanced numerical analysis tools that interpret large datasets, refine and optimize the diagnostic response, and couple directly with plasma simulation codes for forward modeling of diagnostic data. They are useful for validation exercises and the training of advanced prediction/control strategies. A comparison of synthetic diagnostic and

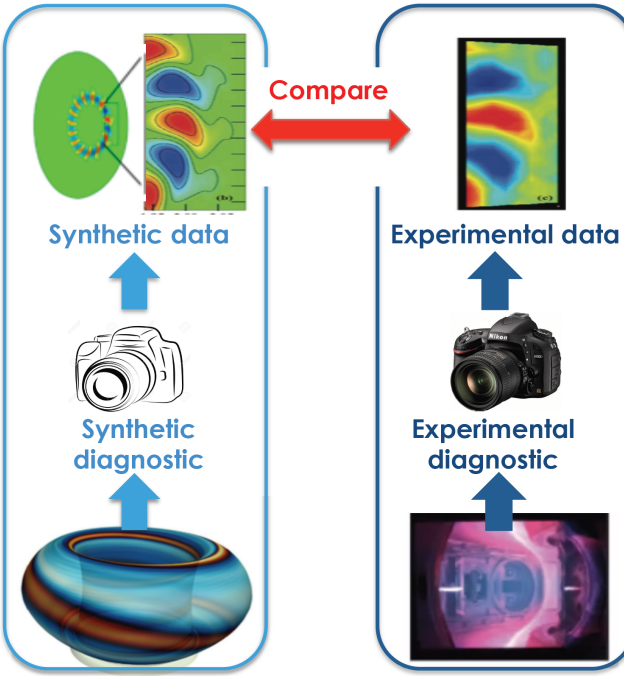


Figure 20. Comparison of the synthetic analysis and experimental approach for fusion plasma data acquisition.

experimental approaches for fusion plasma data acquisition is shown in figure 20. Synthetic diagnostics are invaluable for interpretation of new data from edge regions of high-performance discharges. Fully self-consistent 2D and 3D models of microwave propagation are equally important for optimizing electronic and digital beamforming antenna arrays. Coupling these synthetic diagnostics with plasma simulation codes will inevitably lead to measurement innovation and important new experimental methods. In the foreseeable future, synthetic diagnostic data may even be integrated with machine learning methods such as deep neural networks for the intelligent automation of diagnostic alignment and plasma control.

Synthetic diagnostics support both the design of new systems and the interpretation of new data. Individual synthetic diagnostic modules simulate the response of a given diagnostic (e.g. FWR2D/3D for modeling reflectometry or ECEI2D [60] for modeling cyclotron radiometry [57]). Other modules process the output of plasma simulation codes (e.g. M3D-C1 [80], XGC0 [81], and GTC [82]) to produce background plasma profiles and time-dependent fluctuations. A synthetic diagnostic platform combines these modules so that one can determine how a given diagnostic system will respond to a given plasma behavior. Within the model, that diagnostic can be modified until the synthetic response properly resolves the crucial aspects of the mode structure or plasma behavior—this is how diagnostic design is aided by a synthetic diagnostic platform. Once the diagnostic is installed and has provided data, a comparison of real and synthetic data provides the understanding that is required to interpret complex imaging data. Enhancements to the synthetic diagnostic capability therefore lead to enhanced measurement capability. The scientific benefit of synthetic diagnostics is summarized in figure 21.

5.2. 2D/3D synthetic diagnostic modeling and integration of an open-source platform including equilibrium reconstruction and plasma simulation codes

As shown in figure 22, the synthetic diagnostics analysis couples quasi-optical modeling of the antennas and lens system, plasma simulation codes generating linear and nonlinear time-dependent plasma fluctuations, and 2D/3D full-wave modeling of the plasma-wave interaction at the microwave reflection layer. This capability has been used extensively in the design of MIR diagnostics [58, 59]. Furthermore, it has been used to make a comparison between linear, time-dependent M3D-C1 simulations of the edge harmonic oscillation (EHO) on DIII-D and recently collected MIR data [50]. This comparison has confirmed expectations, that the MIR optical design, characterized in detail during first-ever in-vessel measurements, readily distinguishes the poloidal wavenumber of the mode. Measurement of the mode structure helps to validate the physical picture for EHO stability and control, an important aspect of QH-mode development for ELM avoidance.

In addition to FWR2D/3D codes for modeling reflectometry, a new code, ECEI2D, for modeling ECEI data has been developed [57]. This code implements a first-of-kind self-consistent reciprocal model that includes not only the emission, reabsorption, and radiation transport, but also simultaneously models refraction and diffraction of the quasi-optical imaging system. This new capability allows for realistic forward modeling of the diagnostic response under a variety of conditions and will be enormously valuable for interpreting data from the plasma edge, where optical thickness varies rapidly along with the plasma's refractive index. This code has been incorporated into an open-source Python software package, which includes modules for reading the time-dependent output of plasma simulation codes such as M3D-C1, XGC0, and GTC.

6. Discussion

For initial studies, commercial E-band low-noise GaAs receiver chips, are being employed in the ECEI array upgrade at DIII-D. This will provide valuable data for ITER 15 MA scenario development discharges with toroidal field on axis in the vicinity of 1.7 T. Further IC advancements can similarly benefit other areas, such as QH-mode development for naturally ELM-free operation and advanced tokamak (AT) scenarios, including high poloidal plasma beta, for steady-state operation. However, far greater flexibility is necessary in order to cover all these various operating conditions at DIII-D as well as other major tokamaks, such as W-, F-, and D-band for ECEI (75–110, 90–140 and 110–170 GHz) and V- and W-band for MIR (50–75 and 75–110 GHz). Therefore, designing custom MMICs that are free of the constraints from commercial vendor supplies is the key to enable precise coverage of relevant frequencies for fusion plasmas. Fortunately, in a number of semiconductor foundries, custom IC production can reach beyond 150 GHz (and trending even higher!), and thus may become a driving force in the advancement of fusion plasma diagnostics.

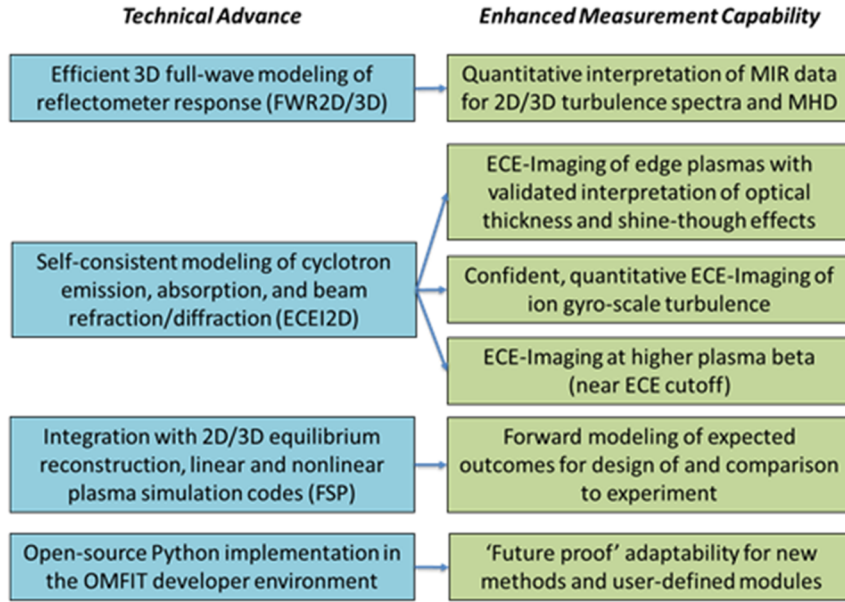


Figure 21. Synthetic diagnostic developments enable unambiguous data interpretation and open-source data analysis.

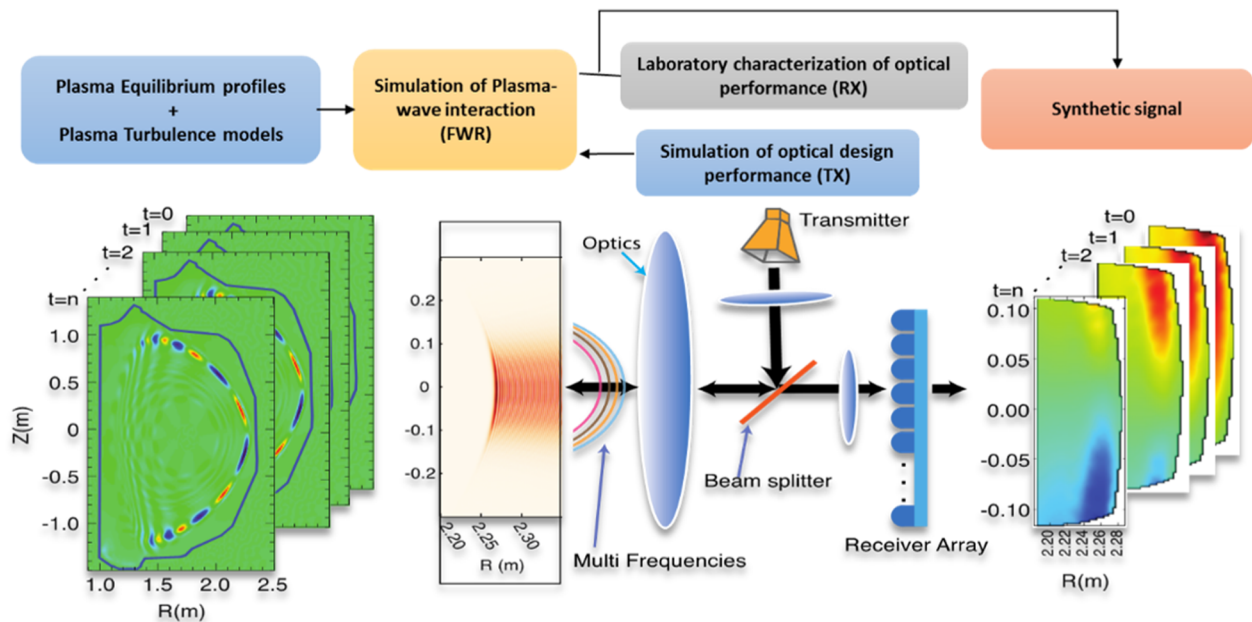


Figure 22. Demonstration of an individual synthetic MIR diagnostic.

In terms of available IC technologies, CMOS is well suited for implementation at frequencies below W-band, because it can support a high level of integration and thus many functionalities. This makes CMOS perfect for MIR applications, including the design of high-power multi-tone transmitters and multi-channel receivers. For higher frequencies from W-band up to 200 GHz and beyond (e.g. F-, D-, and G-band as required by higher field devices such as EAST), III-V semiconductor processes (such as InP and GaN where the wide bandgap of the latter provides thermal robustness and relative immunity to stray RF damage) provide superior performance in terms of significantly lower noise temperature, higher dynamic range, and higher conversion gain. The output

1 dB compression point ($P_{1\text{dB}}$) of a low noise amplifier (LNA) up to G-band is usually around 1 dBm [83, 84]. These LNAs have a typical gain of 15–20 dB [83, 84]. The estimated input power that the LNA by itself can sustain is around -5 dBm to maintain low noise. For Gallium Nitride (GaN) low noise amplifiers, the output $P_{1\text{dB}}$ in W-band is around 25 dBm [85]. GaN devices up to G-band can be biased at drain voltage of $V_d = 10\text{ V}$ and its break down voltage is beyond 20 V [78]. For a GaN low noise amplifier, we expect that the input power can be as high as $\sim 20\text{ dBm}$ in the W-band [85] and $\sim 10\text{ dBm}$ in G-band [78]. However, most of the time, these LNAs can be protected with limiters which are widely used in phased-array antenna systems. For our systems, a number of techniques [2]

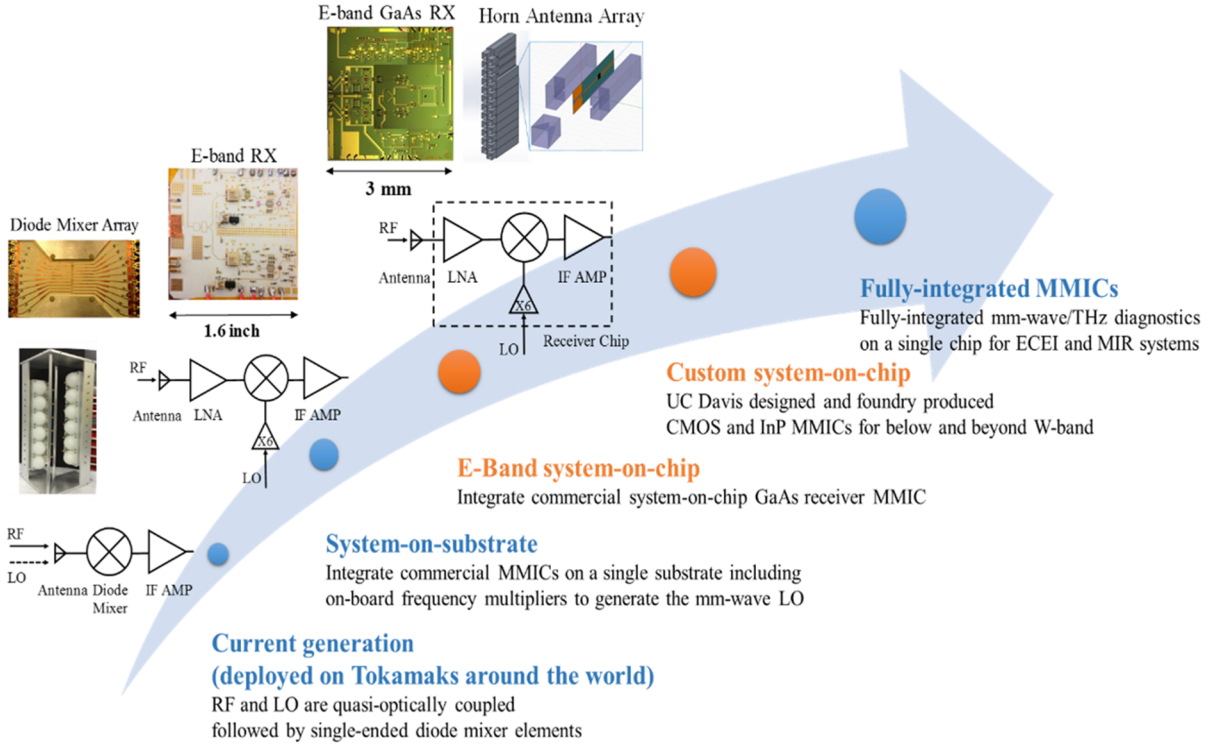


Figure 23. Roadmap for developing state-of-the-art mm-wave IC technologies for fusion plasma imaging. At the end of each development phase, the technology will be transitioned to fusion imaging systems for diagnostics.

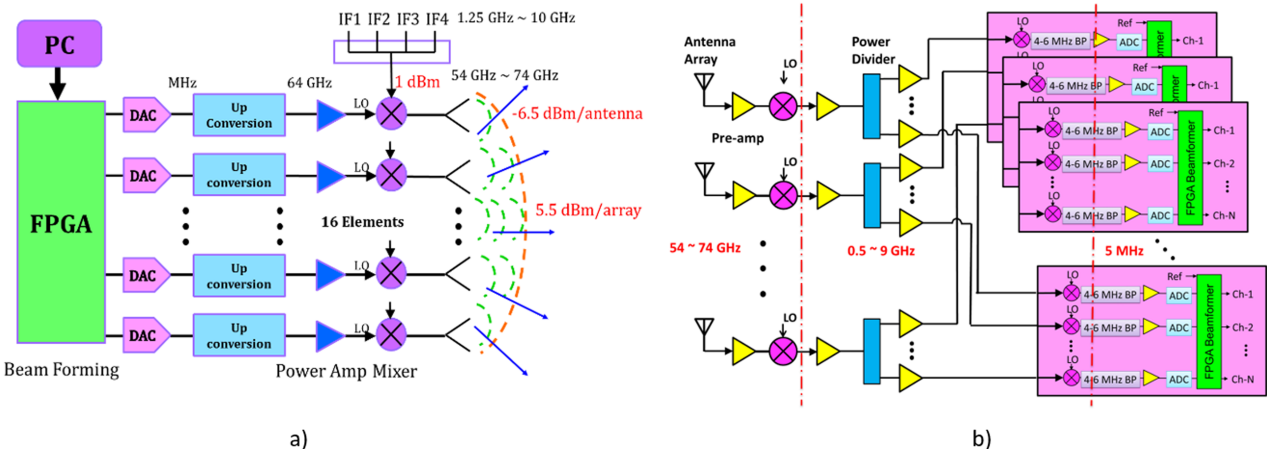


Figure 24. V-band transmitter-receiver architecture with FPGA digital beamforming module. (a) RF transmitter architecture. (b) RF receiver architecture.

such as notch filters (up to 60 dB rejection), novel fuses, and limiters can be used to protect the LNAs. For on-chip or fully integrated circuits, limiters are widely used for protection of receivers. Fortunately, Gallium Nitride and Indium Phosphide (InP) semiconductor devices have been shown to provide high power [78, 86–89]. GaN devices have high breakdown voltage to beyond 20 V while InP can be stacked to provide high voltage. For example, an InP power amplifier can achieve up to 823 mW at 216 GHz by combining a number of 80 mW amplifiers. In the W-band, researchers have demonstrated a 5 W output power GaN power amplifier using combiners [87] and 1 W to 2 W output power from a single MMIC amplifier at W-band [88, 89]. This basically means that these InP and GaN

devices can be used to develop a limiter circuit that can handle a few watts input power to protect the LNA in the W-band and ~1 W in the G-band (up to 220 GHz). For these reasons, we believe InP and GaN technology to be essential for the future of ECE-Imaging.

We envision single chip receivers for ECEI and integrated transceivers for MIR, extending from 50 GHz to 200 GHz and beyond. Highly integrated and unparalleled signal processing capabilities of IC technologies leads to greatly reduced size, power consumption, and cost of reflectometer and radiometer systems, while improving their performance and flexibility. Our roadmap for incorporating state-of-the-art IC transceivers for fusion plasma diagnostics is illustrated in figure 23.

DBF eliminates the need for mechanical alignment of the motor-controlled optical lenses in the current ECEI and MIR systems, which provide focusing for particular plasma conditions essentially only once per discharge. In contrast, microwave diagnostic systems, enabled by the fast processing speed of FPGA and feedback-controlled algorithms, will be capable of automatic alignment with high accuracy between shots or even during a particular discharge to track phenomena of interest.

Currently, FPGA controlled DBFs are being developed for both transmitter and receiver phased arrays. Figure 24(a)) illustrates the overall transmitter architecture, which is comprised of a PC, a FPGA chip, and 16 up-conversion channels. First, a programmable FPGA provides the digital signal with controlled amplitude and phase. Then, a digital-to-analog converter (DAC) changes the signal from the digital to the analog domain. Second, the transmitter MMICs up-convert the signals and transmit them through the antenna array. In this way, multi-frequency phased arrays are realized. The complimentary receiver architecture shown in figure 24(b)) features the same antennas, followed by the receiver MMICs. A second down-conversion stage selects individual cutoff layers within the plasma. Ultimately, custom ICs are incorporated to achieve low-noise temperature, efficient signal processing, and out-of-band interference rejection. Synthetic diagnostic modeling will also provide data for developing the feedback control algorithm for the FPGA.

Acknowledgments

This work is supported by US DoE grants DE-AC02-09CH11466 and DE-FG02-99ER54531. This paper has described our fusion plasma imaging technology developments. Here, we wish to acknowledge A.J.H. Donné, H.K. Park, I.G.J. Classen, T. Munsat, E. Mazzucato, and G.S. Yun, with whom we collaborated with physics measurements using these instruments.

References

- [1] Tobias B.J., Austin M.E., Boom J.E., Burrell K.H., Classen I.G.J., Domier C.W., Luhmann N.C. Jr, Nazikian R. and Snyder P.B. 2012 ECE-imaging of the H-mode pedestal *Rev. Sci. Instrum.* **83** 10E329
- [2] Tobias B. et al 2010 Commissioning of electron cyclotron emission imaging instrument on the DIII-D tokamak and first data *Rev. Sci. Instrum.* **81** 10D928
- [3] Tobias B. et al 2009 Advancements in electron cyclotron emission imaging demonstrated by the TEXTOR ECEI diagnostic upgrade *Rev. Sci. Instrum.* **80** 093502
- [4] Classen I.G.J., Domier C.W., Luhmann N.C. Jr, Bogomolov A.A., Suttrop W., Boom J.E., Tobias B.J., Donné A.J.H. and ASDEX Upgrade Team 2014 Dual array 3D electron cyclotron emission imaging at ASDEX Upgrade *Rev. Sci. Instrum.* **85** 11D833
- [5] Yu L., Domier C.W., Kong X., Che S., Tobias B., Park H., Yu C.X. and Luhmann N.C. Jr 2012 Recent advances in ECE imaging performance *J. Instrum.* **7** C02055
- [6] Munsat T., Park H.K., Classen I.G.J., Domier C.W., Donné A.J.H., Luhmann N.C. Jr, Mazzucato E., van de Pol M.J. and the TEXTOR Team 2007 Localization of the magnetic reconnection zone during sawtooth crashes in tokamak plasmas *Nucl. Fusion* **47** L31–5
- [7] Tobias B. et al 2015 Microwave imaging reflectometry on DIII-D 1st EPS Conf. on Plasma Diagnostics (Frascati, Italy), 14–17 April 2015 (https://pos.sissa.it/archive/conferences/240/004/ECPD2015_004.pdf)
- [8] Tobias B. et al 2011 Recent progress on microwave imaging technology and new physics results *Plasma Fusion Res.* **6** 2106042
- [9] Tobias B. et al 2011 Imaging techniques for microwave diagnostics *Contrib. Plasma Phys.* **51** 2–3
- [10] Muscatello C.M. et al 2014 Technical overview of the millimeter-wave imaging reflectometer on the DIII-D tokamak *Rev. Sci. Instrum.* **85** 11D702
- [11] Muscatello C.M., Domier C.W., Hu X., Luhmann N.C. Jr, Ren X., Riemschneider P., Spear A., Yu L. and Tobias B. 2014 Multidimensional visualization of MHD and turbulence in fusion plasmas *IEEE Trans. Plasma Sci.* **42** 2734–5
- [12] Hsia R.P., Geck W.R., Cheng S., Zhang W.-M., Domier C.W. and Luhmann N.C. Jr 1995 ECE imaging array diagnostic development of TEXT-U *Rev. Sci. Instrum.* **66** 834
- [13] Cima G., Deng B., Domier C.W., Geck W.R., Hsia R.P., Liang C., Jiang F., Luhmann N.C. Jr and Brower D. 1997 ECE imaging on TEXT-U *Fusion Eng. Des.* **34–5** 515–8
- [14] Deng B.H., Brower D.L., Cima G., Domier C.W., Luhmann N.C. Jr and Watts C. 1998 Mode structure of turbulent electron temperature fluctuations in the Texas Experimental Tokamak Upgrade *Phys. Plasmas* **5** 4117
- [15] Cima G., Gentle K.W., Wootton A., Brower D.L., Zeng L., Deng B.H., Domier C.W. and Luhmann N.C. Jr 1998 Electron heat diffusivity in the sawtooth tokamak core *Plasma Phys. Control. Fusion* **40** 1149
- [16] Deng B.H., Hsia R.P., Domier C.W., Burns S.R., Hillyer T.R., Luhmann N.C. Jr, Oyevar T., Donné A.J.H. and RTP Team 1999 Electron cyclotron emission imaging diagnostic system for Rijnhuizen Tokamak Project *Rev. Sci. Instrum.* **70** 998
- [17] Deng B.H., Domier C.W., Luhmann N.C. Jr, Brower D.L., Cima G., Donné A.J.H., Oyevar T. and van de Pol M.J. 2001 ECE imaging of electron temperature and electron temperature fluctuations (invited) *Rev. Sci. Instrum.* **72** 301
- [18] Munsat T., Mazzucato E., Park H., Deng B.H., Domier C.W., Luhmann N.C. Jr, Wang J., Xia Z.G., Donné A.J.H. and van de Pol M. 2003 Microwave imaging reflectometer for TEXTOR (invited) *Rev. Sci. Instrum.* **74** 1426
- [19] Park H. et al 2003 Recent advancements in microwave imaging plasma diagnostics *Rev. Sci. Instrum.* **74** 4239
- [20] Park H. et al 2004 Simultaneous microwave imaging system for density and temperature fluctuation measurements on TEXTOR (invited) *Rev. Sci. Instrum.* **75** 3787
- [21] Mazzucato E. 2001 Microwave imaging reflectometry for the visualization of turbulence in tokamaks *Nucl. Fusion* **41** 203
- [22] Mazzucato E., Munsat T., Park H., Deng B.H., Domier C.W., Luhmann N.C. Jr, Donné A.J.H. and van de Pol M.J. 2002 Fluctuation measurements in tokamaks with microwave imaging reflectometry *Phys. Plasmas* **9** 1955
- [23] Nazikian R. and Mazzucato E. 1995 Reflectometer measurements of density fluctuations in tokamak plasmas (invited) *Rev. Sci. Instrum.* **66** 392
- [24] Classen I.G.J. et al 2010 2D electron cyclotron emission imaging at ASDEX Upgrade (invited) *Rev. Sci. Instrum.* **81** 10D929
- [25] Liang T., Tobias B., Kong X., Domier C.W., Luhmann N.C. Jr, Lee W., Yun G.S. and Park H.K. 2010 Innovations in optical coupling of the KSTAR electron cyclotron emission imaging diagnostic *Rev. Sci. Instrum.* **81** 10D909
- [26] Yun G.S. et al 2010 Development of KSTAR ECE imaging system for measurement of temperature fluctuations and edge density fluctuations *Rev. Sci. Instrum.* **81** 10D930

- [27] Xu M. *et al* 2011 Electron cyclotron emission imaging on the EAST tokamak *Plasma Sci. Technol.* **13** 167
- [28] Luo C. *et al* 2014 Quasi-optics design of the dual-array ECE imaging system on the EAST Tokamak *J. Instrum.* **9** 12
- [29] Domier C. *et al* 2011 Wide radial coverage electron cyclotron emission imaging (ECEI) system for EAST *53rd Annual Meeting of the APS Division of Plasma Physics (Utah, USA, 14–18 November 2011)* vol 56 (<http://meetings.aps.org/Meeting/DPP11/Event/153249>) no. 16
- [30] Zhu Y. *et al* 2016 The general optics structure of millimeter-wave imaging diagnostic on tokamak *J. Instrum.* **11** P01004
- [31] Xu M. *et al* 2013 Internal magnetic configuration measured by ECE imaging on EAST tokamak *Plasma Sci. Technol.* **15** 1189
- [32] Hussain A. *et al* 2015 Electron cyclotron emission imaging observations of $m/n = 1/1$ and higher harmonic modes during sawtooth oscillation in ICRF heating plasma on EAST *Chin. Phys. Lett.* **32** 065201
- [33] Hussain A. *et al* 2016 Observations of compound sawteeth in ion cyclotron resonant heating plasma using ECE imaging on experimental advanced superconducting tokamak *Phys. Plasmas* **23** 042504
- [34] Zhu Y. *et al* 2014 Optics design for J-TEXT ECE imaging with field curvature adjustment lens *Rev. Sci. Instrum.* **85** 11D854
- [35] Pan X.M. *et al* 2016 Design of the 2D electron cyclotron emission imaging instrument for the J-TEXT tokamak *Rev. Sci. Instrum.* **87** 11E106
- [36] Ma X.D. *et al* 2016 Optics design for electron cyclotron emission imaging system on J-TEXT *J. Instrum.* **11** P05022
- [37] Jiang M. *et al* 2013 Development of electron cyclotron emission imaging system on the HL-2A tokamak *Rev. Sci. Instrum.* **84** 113501
- [38] Shi Z. *et al* 2014 Development of microwave imaging reflectometry on the HL-2A tokamak *Rev. Sci. Instrum.* **85** 11D816
- [39] Jiang M., Shi Z., Ding X., Liu Z., Li J., Zhong W., Chen W. and Yang Q. 2013 Development of 24×8 electron cyclotron emission imaging (ECEI) diagnostic system on HL-2A tokamak *16th Chinese Conf. on Plasma Physics and Technology (Shanghai, 2013)* (www.cstam.org.cn/templates/lxzh_1/index.aspx?nodeid=65&page=ContentPage&contentid=172418)
- [40] Tobias B.J., Classen G.J., Domier C.W., Heidbrink W.W., Luhmann N.C. Jr, Naikian R., Park H.K., Spong D.A. and Van Zeeland M.A. 2011 Fast ion induced shearing of 2D Alfvén eigenmodes measured by electron cyclotron emission imaging *Phys. Rev. Lett.* **106** 075003
- [41] Tobias B.J., Austin M.E., Boom J.E., Classen I.G.J., Domier C.W., Luhmann N.C. Jr, Nazikian R. and Yu L. 2012 Intense millimeter wave radiation from the h-mode pedestal in DIII-D at ITER relevant collisionality *39th EPS Conf. on Plasma Physics 2012, EPS 2012 and the 16th Int. Congress on Plasma Physics (Stockholm 2–6 July, 2012)* (<https://www.scopus.com/inward/record.uri?eid=2-s2.0-84876903828&partnerID=40&md5=380aeb79867a735fb8dacc822943b2d1>)
- [42] Yu L., Domier C.W., Luhmann N.C. Jr, Tobias B.J., Solomon W.M. and Austin M.F. 2013 Intense bursts of millimeter-wave emission in QH-mode plasmas on the DIII-D tokamak *55th Annual Meeting of the APS Division of Plasma Physics (Denver, Colorado, USA, 11–15 November 2013;)* vol 58 (<http://meetings.aps.org/Meeting/DPP13/Session/BP8.94>) no. 16
- [43] Fuchs C. and Austin M.E. 2001 Measurements of edge-localized-mode induced electron cyclotron emission bursts in DIII-D *Phys. Plasmas* **8** 1594–9
- [44] Austin M.E., Wu S.M., Harvey R.W. and Ellis R.F. 2006 Investigation of Narrowband ECE Bursts in DIII-D *Plasmas Proc. of the 14th Joint Workshop on Electron Cyclotron Heating and Electron Cyclotron Resonance Heating (Santorini island, Greece, 9–12 May 2006)* (http://ec14.conferences.gr/fileadmin/dtemplates/ec14/latest_abstracts/34.pdf) (<https://fusion.gat.com/pubs-int/MISCONF06/A25479.pdf>)
- [45] Freethy S.J. *et al* 2015 Electron kinetics inferred from observations of Microwave bursts during edge localized modes in the mega-amp spherical tokamak *Phys. Rev. Lett.* **114** 125004
- [46] Rozhdestvensky V.V. *et al* 2015 Nonthermal microwave emission features under the plasma ohmic heating and low-hybrid current drive in the FT–2 tokamak *Energy Environ. Eng.* **3** 42–9
- [47] Freethy S., Shevchenko V., Huang B. and Vann R. 2015 Localised microwave bursts during ELMs on MAST *EPJ Web of Conf.* **87** 03008
- [48] Vianello N. *et al* 2011 Direct observation of current in Type-I edge-localized-mode filaments on the ASDEX Upgrade Tokamak *Phys. Rev. Lett.* **106** 125002
- [49] Yun G.S., Lee W., Choi M.J., Lee J., Park H.K., Tobias B., Domier C.W., Luhmann N.C. Jr, Donné A.J.H., Lee J.H. and the KSTAR Team 2011 Two-dimensional visualization of growth and burst of the edge-localized filaments in KSTAR H-mode plasmas *Phys. Rev. Lett.* **107** 045004
- [50] Ren X., Chen M., Chen X., Domier C.W., Ferraro N.M., Kramer G.J., Luhmann N.C. Jr, Muscatello C.M., Nazikian R. and Shi L. 2015 Microwave imaging reflectometry for the study of edge harmonic oscillations on DIII-D *JINST* **10** P10036
- [51] Luhmann N.C. Jr, Bindsley H., Park H., Sanchez J., Taylor G. and Yu C.X. 2008 Chapter 3 microwave diagnostics *Fusion Sci. Technol.* **53** 335–96
- [52] Kuwahara D., Tseji-Ilo S., Nagayama Y., Yoshinaga T., Sugito M., Shi Z., Yamaguchi S., Kogi Y. and Mase A. 2009 Development of 2D antenna array for microwave imaging reflectometry in LHD *J. Plasma Fusion Res. Ser.* **8** 649–54 (www.jspf.or.jp/JPFRS/PDF/Vol8/jpfrs2009_08-0649.pdf)
- [53] Kuwahara D., Tsuji-Ilo S., Nagayama Y., Yoshinaga T., Shi Z., Yamaguchi S., Sugito M., Kogi Y. and Mase A. 2020 Upgrade of 2D antenna array for microwave imaging reflectometry and ECE imaging *J. Plasma Fusion Res. Ser.* **9** 125–30 (www.jspf.or.jp/JPFRS/PDF/Vol9/jpfrs2010_09-125.pdf)
- [54] Kuwahara D., Ito N., Nagayama Y., Yoshinaga T., Yamaguchi S., Yoshikawa M., Kohagura J., Sugito S., Kogi Y. and Mase A. 2014 Development of horn antenna mixer array with internal local oscillator module for microwave imaging diagnostics *Rev. Sci. Instrum.* **85** 11D805
- [55] Kuwahara D., Ito N., Nagayama Y., Tsuchiya H., Yoshikawa M., Kohagura J., Yoshinaga T., Yamaguchi S., Kogi Y. and Mase A. 2015 Development of local oscillator integrated antenna array for microwave imaging diagnostics *JINST* **10** C12031
- [56] Ren X., Domier C.W., Kramer G., Luhmann N.C. Jr, Muscatello C.M., Shi L., Tobias B.J. and Valeo E. 2014 Process to generate a synthetic diagnostic for microwave imaging reflectometry with the full-wave code FWR2D *Rev. Sci. Instrum.* **85** 11D863
- [57] Shi L., Valeo E.J., Tobias B.J., Kramer G.J., Hausammann L., Tang W.M. and Chen M. 2016 Synthetic diagnostics platform for fusion plasmas *Rev. Sci. Instrum.* **87** 11D303
- [58] Ren X., Tobias B.J., Che S., Domier C.W., Luhmann N.C. Jr, Muscatello C.M., Kramer G. and Valeo E. 2012 Evaluation of the operating space for density fluctuation measurements employing 2D imaging reflectometry *Rev. Sci. Instrum.* **83** 10E338

- [59] Lei L., Tobias B., Domier C.W., Luhmann N.C. Jr., Kramer G.J., Valeo E.J., Lee W., Yun G.S. and Park H.K. 2010 A synthetic diagnostic for the evaluation of new microwave imaging reflectometry diagnostics for DIII-D and KSTAR *Rev. Sci. Instrum.* **81** 10D904
- [60] Valeo E.J., Kramer G.J. and Nazikian R. 2002 Two-dimensional simulations of correlation reflectometry in fusion plasmas *Plasma Phys. Control. Fusion* **44** L1–10
- [61] LaBombard B., Marmar E., Irby J., Terry J.L., Vieira R., Wallace G., Whyte D.G., Wolfe S., Wukitch S. and Baek S. 2015 ADX: a high field, high power density, advanced divertor and RF tokamak *Nucl. Fusion* **55** 053020
- [62] Kessel C.E., Koechl F. and Kim S.H. 2015 Examination of the entry to burn and burn control for the ITER 15 MA baseline and hybrid scenarios *Nucl. Fusion* **55** 063038
- [63] Casper T., Gribov Y., Kavin A., Lukash V., Khayrutdinov R., Fujieda H. and Kessel C. 2013 Development of the ITER baseline inductive scenario *Nucl. Fusion* **54** 013005
- [64] Burrell K.H. et al 2001 Quiescent double barrier high-confinement mode plasmas in the DIII-D tokamak *Phys. Plasmas* **8** 2153
- [65] Garofalo A.M., Solomon W.M., Park J.K., Burrell K.H., DeBoo J.C., Lanctot M.J., McKee G.R., Reimerdes H., Schmitz L. and Schaffer M.J. 2011 Advances towards QH-mode viability for ELM-stable operation in ITER *Nucl. Fusion* **51** 083018
- [66] Chen X., Burrell K.H., Ferraro N.M., Osborne T.H., Austin M.E., Garofalo A.M., Groebner R.J., Kramer G.J., Luhmann N.C. Jr and McKee G.R. 2016 Rotational shear effects on edge harmonic oscillations in DIII-D quiescent H-mode discharges *Nucl. Fusion* **56** 076011
- [67] Scheytt J.C., Sun Y., Beer S., Zwisch T. and Kaynak M. 2011 Mm-wave system-on-chip & system-in-package design for 122 GHz radar sensors *12th Int. Symp. on RF MEMS and RF Microsystems (Athens, Greece, 27–29 June 2011)*
- [68] Feger R. and Stelzer A. 2015 Millimeter-wave radar systems on-chip and in package: current status and future challenges *IEEE Topical Conf. on Wireless Sensors and Sensor Networks (WiSNet) (San Diego, CA, 25–28 January 2015)* (<https://doi.org/10.1109/WISNET.2015.7127407>)
- [69] Tobias B., Domier C.W., Luhmann N.C. Jr., Luo C., Mamidanna M., Phan T., Pham A.-V. and Wang Y. 2016 Low-noise heterodyne receiver for electron cyclotron emission imaging and microwave imaging reflectometry *Rev. Sci. Instrum.* **87** 11E103
- [70] Chieh J.C., Pham A.-V., Pidwerbestsky A. and Kannell G. 2013 A low cost 8 × 8 W-Band substrate integrated waveguide antenna array detector on LCP *Microw. Opt. Technol. Lett.* **55** 1825–30
- [71] Chen M.J., Pham A., Evers N.A., Kapusta C., Iannotti J., Kornrumpf W., Maciel J. and Karabudak N. 2006 Design and development of a package using LCP for RF/Microwave MEMS switches *IEEE Trans. Microw. Theory Tech.* **54** 4009–15
- [72] Chen M., Evers N., Kapusta C., Iannotti J., Kornrumpf W., Pham A., Maciel J. and Karabudak N. 2007 Reliability of a hermetic LCP package for RF MEMS switches *Proc. GOMAC (Lake Buena Vista, FL, 19–22 March 2007)*
- [73] McGrath M.P., Aihara K., Pham A. and Nelson S. 2008 Development of LCP surface mount package with a bandpass feedthrough at K-band *IEEE Int. Microwave Symp. (Atlanta, GA, USA, 2008)* (<https://doi.org/10.1109/MWSYM.2008.4633111>)
- [74] Pham A.-V., Chen M.J. and Aihara K. 2012 *LCP for Microwave Packages and Modules* (Cambridge: Cambridge University Press)
- [75] Cima G. 1994 Correlation properties of black-body radiation in the context of the electron cyclotron emission of a magnetized plasma *Il Nuovo Cimento D* **16** 359–64
- [76] Freethy S.J. et al 2016 Measurement of turbulent electron temperature fluctuations on the ASDEX Upgrade tokamak using correlated electron cyclotron emission *Rev. Sci. Instrum.* **87** 11E102
- [77] Shen Z. et al 2007 Protection filters in ECEI systems for plasma diagnostics *Plasma Fusion Res.* **2** S1030
- [78] Margomenos A. et al 2014 GaN technology for E, W, and G-band applications *Compound Semiconductor Integrated Circuit Symp. (CSICs), 2014 IEEE San Diego, California, USA, 19–22 October 2014* (<https://doi.org/10.1109/CSICS.2014.6978559>)
- [79] Chang Y.T., Ye Y., Gu G.J., Domier C.W. and Luhmann N.C. Jr 2016 The V-band CMOS multi-frequency transmitter for plasma imaging radar reflectometric diagnostics *IEEE MTT-S Int. Microwave Symp. (IMS) (San Francisco, CA, 22–27 May 2016)* (<https://doi.org/10.1109/MWSYM.2016.7540361>)
- [80] Ferraro N.M., Jardin S.C. and Snyder P.B. 2010 Ideal and resistive edge stability calculations with M3D-C *Phys. Plasmas* **17** 102508
- [81] Ku S., Baek H. and Chang C.S. 2004 Property of an XX-point generated velocity-space hole in a diverted tokamak plasma edge *Phys. Plasmas* **11** 5626
- [82] Lin Z., Hahm T.S., Lee W.W., Tang W.M. and White R.B. 1998 Turbulent transport reduction by zonal flows: massively parallel simulations *Science* **281** 1835–7
- [83] OMMIC III-V product information OMMIC (Online) (www.ommic.com/)
- [84] Kangaslahti P., Pukala D., Gaier T., Deal W., Mei X. and Lai R. 2008 Low noise amplifier for 180 GHz frequency band *IEEE Int. Microwave Symp. (Atlanta, USA, 2008)*
- [85] Masuda S. et al 2009 GaN MMIC amplifiers for W-band transceivers *European Microwave Integrated Circuits Conf. (Rome, Italy, 28–29 September 2009)* (<http://ieeexplore.ieee.org/document/5296076/>)
- [86] Rollin J. et al 2015 A PolyStrata 820 mW G-band solid state power amplifier *IEEE Compound Semiconductor Integrated Circuit Symp. (New Orleans, USA, 11–14 October 2015)* (<https://doi.org/10.1109/CSICS.2015.7314481>)
- [87] Schellenberg J., Watkins E., Micovic M., Kim B. and Kyu Han H. 2010 W-band, 5 W solid-state power amplifier/combiner *IEEE MTT-S Int. Microwave Symp. Digest (MTT) (Anaheim, CA, USA, 23–28 May 2010)* (<https://doi.org/10.1109/MWSYM.2010.5517616>)
- [88] Brown A., Brown K., Chen J., Hwang K.C., Kolias N. and Scott R. 2011 W-band GaN power amplifier MMICs *IEEE MTT-S Int. Microwave Symp. Digest (MTT) (Baltimore, MD, USA, 5–10 June 2011)* (<https://doi.org/10.1109/MWSYM.2011.5972571>)
- [89] Schellenberg J., Kim B. and Phan T. 2013 W-Band, broadband 2W GaN MMIC *IEEE Int. Microwave Symp. (IMS) (Seattle, WA, USA, 2013)* (<https://doi.org/10.1109/MWSYM.2013.6697656>)